Genotype-phenotype correlations in Wilms tumor initiation

N.S. Pop[1], D. Koot[1], C.M. Brouwers[2], M.M. Linssen[2], J.W.C. Claassens[2], C.W.J. Cartlidge[3], D.D. Özdemir[3], K.S. Dolt[1,3], P. Hohenstein[1,2,3,4,*]

[1]Department of Human Genetics, Leiden University Medical Center, Leiden, Netherlands

[2]Transgenic Facility Leiden, Central Animal Facility, Leiden University Medical Center, Leiden, Netherlands

[3]Division of Developmental Biology, The Roslin Institute, Edinburgh, United Kingdom

[4]Lead contact

* Correspondence: p.hohenstein@lumc.nl

Summary

Wilms tumor, the most common pediatric kidney cancer, arises from abnormal embryonic kidney development. Therapy resistance and tumor recurrence remain major challenges, likely driven by the presence of Cancer Stem Cells (CSCs). Here, we elucidate the earliest pathogenic events in genomically engineered mouse models exhibiting loss of *Wt1* or *LIN28B* overexpression, two Wilms tumor driver genes. Loss of *Wt1* causes a spatially and temporarily lineage-specific phenotype, with the first blastemal-like cells appearing in combined nephrogenic and stromal conditional loss of *Wt1*. In contrast, *LIN28B* overexpression leads to postnatal blastemal overgrowth with presence of cells co-expressing the Ncam1, Aldh1a2, Six2, and Cited1 CSC markers, suggesting a mixed and unstable uninduced/induced blastemal population, and revealing cellular heterogeneity within early tumors. Our findings demonstrate a detailed framework of the earliest pathogenic events, and corresponding cancer stem cell marker expression patterns, driven by biologically distinct mutated genes.

Highlights and eTOC blurb

1. Lineage-specific *Wt1* loss shows spatially and temporally distinct phenotypes.

2. Early loss of Wt1 delays nephrogenesis and triggers early blastemal expansion.

3. LIN28B overexpression expands NPCs which induce postnatal blastemal overgrowth.

4. LIN28B overexpression yields blastema co-expressing four CSC markers.

eTOC Blurb (<60 words)

In this study, Pop and colleagues dissect the lineage-specific functions of Wt1 and LIN28B during kidney development. Using conditional mouse models, they show that Wt1 loss depending on the spatial and temporal context blocks nephrogenesis, while LIN28B overexpression expands progenitor-like populations, marked as blastemal-like cells, co-express the four established CSC markers. These findings highlight initial steps of Wilms tumorigenesis.

38 ## Introduction

39

40 Wilms tumor is the most common pediatric renal malignancy, occurring in approximately 1 in
41 10,000 children, typically before the age of five (Spreafico et al., 2021). They arise from aberrant
42 embryonic kidney development, potentially during the critical window of definitive kidney
43 development between the fifth and eight week of gestation (Zheng et al., 2023). Standardized
44 diagnostic and therapeutic procedures have made it possible to cure nearly 90% of the affected
45 children. However, therapy resistance, postoperative recurrence, and high-risk Wilms tumors
46 remain significant clinical challenges. Histological analyses consistently reveal persistence of
47 embryonic renal structures within tumors (Beckwith et al., 1990; Hohenstein et al., 2015),
48 including a subset of tumor cells resembling progenitor-like cells. These observations are
49 consistent with the cancer stem cell (CSC) model, in which a small population of stem-like cells
50 drives tumor initiation, recurrence, and therapy resistance, potentially explaining the poor
51 outcomes observed in high-risk Wilms tumor (Bonnet and Dick, 1997; Ginestier et al., 2007;
52 Pode-Shakked et al., 2013). Understanding the origin of these Wilms tumor CSCs would provide
53 valuable insights in the biology of WT and the earliest pathogenic events driving Wilms tumor
54 formation, thus providing new leads to improve patient prognosis and develop targeted
55 therapies.

56 To date, 46 Wilms tumor predisposition and driver genes have been identified, many of
57 which are essential for embryonic kidney development (Spreafico *et al.*, 2021). Among them,
58 Wilms Tumor 1 (*WT1*) is the most extensively studied. Although best known as a transcription
59 factor, WT1 can bind both RNA and DNA, functioning as either an activator or repressor
60 depending on the cellular and chromatin context (Essafi et al., 2011; Hohenstein and Hastie,
61 2006). During nephrogenesis, WT1 is critical for driving mesenchymal-to-epithelial transition
62 (MET) in nephron progenitor cells (NPCs). Approximately 15% of patients carry loss-of-function
63 *WT1* mutations, which are frequently associated with ectopic tissue differentiation into skeletal

64 muscle, fat, and less commonly bone or cartilage (Miyagawa et al., 1998; Schumacher et al.,
65 2003).

66 Another Wilms tumor driver gene, *LIN28B*, is primarily expressed in progenitor cells,
67 where it promotes proliferation and blocks differentiation by inhibiting maturation of the let-7
68 microRNAs, thereby upregulating oncogenic targets including *RAS*, *MYC*, and *HMGA2*
69 (Viswanathan and Daley, 2010). LIN28B has been implicated in tumor progression, epithelial-to-
70 mesenchymal transition, CSC formation, and therapy resistance (Cotino-Najera et al., 2024; Li
71 et al., 2019; Zhou et al., 2013). Its precise role in kidney development is unclear, its declining
72 expression by embryonic day (E)16.5 suggests a temporally restricted function during
73 nephrogenesis (Viswanathan and Daley, 2010; Yermalovich et al., 2019). The earliest phenotypic
74 events following *WT1* loss or *LIN28B* overexpression in Wilms tumor patients remain largely
75 unknown, limiting our understanding of how these mutations initiate tumorigenesis.

76 Several studies defined the Wilms tumor CSC in patient-derived material (Petrosyan et
77 al., 2023; Pode-Shakked *et al.*, 2013). NCAM1^{+} cells with high ALDH activity were found capable
78 of initiating xenograft tumors, fulfilling key CSC criteria, although these cells lost tumorigenic
79 potential when cultured *ex vivo* (Pode-Shakked et al., 2009; Pode-Shakked *et al.*, 2013). More
80 recently a SIX2^{+}CITED1^{+} population was described as a different kind of CSC, maintaining tumor-
81 initiating capacity in culture and meeting the CSC criteria (Petrosyan *et al.*, 2023).

82 These identified CSC markers have distinct functions during normal embryonic kidney
83 development. Polysialylated NCAM1 (PSA-NCAM1), the embryonic version of the neural cell
84 adhesion molecule 1 (NCAM1), is an important protein that mediates cell-cell adhesion, is
85 expressed on NPCs and endothelial cells and facilitates cell movement during kidney
86 development (Niculovic et al., 2025). The protein is expressed in undifferentiated metanephric
87 mesenchyme at E11.5-E12.5 and in early nephron structures (comma- and S-shaped bodies)
88 during kidney development, but is absent postnatally (Markovic-Lipkovski et al., 2007). *Ncam1*-
89 deficient mice exhibit impaired glomerular vascularization, with reduced endothelial cell

numbers and smaller glomeruli, indicating an essential role for NCAM1 in kidney vascularization in the mouse embryonic kidney (Niculovic *et al.*, 2025). ALDH activity, measurable using the ALDEFLUOR assay, is a widely used CSC marker (Ginestier *et al.*, 2007). Multiple ALDH isoforms contribute to this signal, including ALDH1A1, ALDH1A2, ALDH1A3 and ALDH2 (Zhou et al., 2019). ALDH enzymes synthesize retinoic acid from retinaldehyde, a critical signaling molecule that regulates cell differentiation, proliferation, and tissue patterning (Niederreither et al., 1999). Expression is lineage- and stage-specific: *Aldh1a1* and *Aldh1a3* are dynamically expressed in differentiating tubular structures derived from the nephrogenic lineage or ureteric bud, whereas *Aldh1a2* is mainly localized in the cortical stroma and essential for ureteric bud outgrowth and nephron formation, and is weakly expressed in the early nephron (comma- and S-shaped bodies, and in the glomerulus) (Li et al., 2020; Li et al., 2017).

Transcription factors *Six2* and *Cited1* mark uninduced NCPs (Kobayashi et al., 2008; Mugford et al., 2009). Upon NPCs induction, *Cited1* expression is lost first, followed by *Six2* (Mugford *et al.*, 2009). The persistence of SIX2$^+$CITED1$^+$ populations in Wilms tumor xenografts suggests that these tumors may originate from nephron progenitors that failed to undergo proper differentiation, although this developmental process has yet to be conclusively demonstrated. The normal expression pattern of these CSC markers suggest that NCAM1$^+$ALDH-activity is a natural occurrence in early nephron structures (comma- and S-shaped bodies), whereas SIX2$^+$CITED1$^+$ reflects a transcriptional signature of uninduced NPCs.

Genetically engineered mouse models provide a powerful model to study the earliest phenotypic effects of tumor-initiating mutations in a controlled developmental context. These models allow us to track emergence, expansion, and behavior of progenitor-like cell populations that could act as CSCs. Therefore, we use lineage specific loss of *Wt1* and *LIN28B* overexpression mouse models to study the genotype-phenotype correlations during kidney development, and their effects on CSC marker expression.

115 ## Results

116

117 ### Conditional Wt1 knockout models

118 We previously knocked out *Wt1* at different stages of nephron development using *Nes*-Cre, *Pax8*-
119 Cre a *Wnt4*-Cre drivers, showing that the earliest, pre-MET loss of *Wt1* using *Nes*-Cre most
120 closely resembled *WT1*-mutant tumors. It lead to an expansion of mesenchyme and a block of
121 MET (Berry et al., 2015). The metanephric mesenchyme gives rise to the condensed mesenchyme
122 containing the nephron progenitor cells (NPCs), expressing *Six2* (Kobayashi *et al.*, 2008), and the
123 remaining uncondensed mesenchyme containing stromal progenitor cells with a distinct
124 expression pattern of *Foxd1* (Kobayashi et al., 2014). Both populations transiently express *Wt1*
125 (Armstrong et al., 1993; Berry *et al.*, 2015; Weiss et al., 2020). The *Nes*-Cre model affects both
126 lineages, and therefore cannot distinguish between the roles of *Wt1* in them. To determine the
127 nephrogenic- and stromal-specific effects when *Wt1* is lost, we used three Cre-drivers: *Six2*$^{GFPCre-}$
128 $^{IRES-PuroR}$ (*Six2*^{GCiP}) to target the nephrogenic lineage, *Foxd1*^{GFPCre} (*Foxd1*^{GC}) to target the stromal
129 lineage, and *Wt1*^{CreERT2} (*Wt1*^{CE}) for targeting both lineages in a tamoxifen-dependent controlled
130 manner (Dolt et al., 2013; Kobayashi *et al.*, 2014; Zhou et al., 2008). We crossed the three Cre-
131 drivers with the *Wt1* conditional allele (Martinez-Estrada et al., 2010) and in some case included
132 the lox-stop-lox tdTomato reporter (Madisen et al., 2010) to follow the lineage of mutant and
133 control cells. This conditional *Wt1* knockout model is a phenocopy of the conventional
134 model(Kreidberg et al., 1993) when driven by a germline Cre deleter strain, and does not have a
135 phenotype when driven by the *Hoxb7*-Cre ureteric bud-specific driver (Berry *et al.*, 2015).

136

137 ## *Six2*-driven Wt1 loss blocks nephrogenesis

138 To selectively delete *Wt1* in the nephrogenic lineage, we used the *Six2*^{GCiP} driver to knockout *Wt1*
139 in the developing kidney (Fig. 1A). *Six2* is expressed in NPCs from E10.5 in the metanephric
140 mesenchyme and later in the cap mesenchyme, and is predicted to be a direct transcriptional
141 target of *Wt1*(Kobayashi *et al.*, 2008; O'Brien et al., 2018). As NPCs form pretubular aggregates
142 (PTA), which epithelializes into a renal vesicles (RV), comma-shaped and S-shaped bodies to
143 form a mature nephron (McMahon, 2016), *Six2* expression is lost.

144 *Ex vivo* kidney organ culture time lapse imaging of the *Six2*^{GCiP} allele (Dolt *et al.*, 2013) in
145 control E12.5 embryonic kidneys confirmed *Six2*-linked GFP expression in the cap mesenchyme,
146 and the tdTomato lineage reporter confirmed contribution to the nephrogenic lineage, with
147 exclusion from the stroma and ureteric bud (Fig. 1B, left panel; supplementary movie 1A). In
148 contrast, e*x vivo* kidney organ cultures of E12.5 *Six2*^{GCiP} driven *Wt1*-mutant kidneys showed
149 severely disrupted nephron differentiation and ureteric bud branching morphogenesis (Fig. 1B,
150 right panel; supplementary movie 1B). At 0hrs, the *Wt1*-mutant eGFP expressing cells
151 surrounded the ureteric bud tip, but subsequently the eGFP signal decreased, indicative of cells
152 losing SIX2-expression, consistent with *Six2* as potential *Wt1* target (O'Brien *et al.*, 2018). The
153 tdTomato-expressing mutant cells accumulated around the ureteric bud tip, or migrated rapidly
154 outwards. Whole mount immunohistochemical staining confirmed loss of SIX2 in the tdTomato-
155 expressing cells (Fig. 1C).

156 Consistent with the time lapse imaging, histological analysis of E12.5 embryos showed
157 ureteric bud tips surrounded by mesenchymal-like cells (Fig. 1D). Immunohistochemistry
158 confirmed loss of SIX2 expression in tdTomato-expressing cells (Fig. 1E, top panels), which had
159 lost WT1 expression and surrounded a CDH1-positive tubular structure (Fig. 1E, bottom panels).
160 Surrounding stroma, negative for tdTomato, continued to express WT1. Proliferative marker KI67
161 is reduced in the kidney region (Sup. Fig. 5A-B).

162 At E18.5, mutants exhibited structures resembling early budding stage. Sectioning the
163 isolated urogenital system complicated the identification of the kidney remnants in 2D, due to
164 their lower localization in the embryo (Fig. 1F, arrows). The derived structures were negative for
165 SIX2, WT1, and CDH1 expression, making it difficult to define their developmental stage, cellular
166 identity, or structural nature. Nevertheless, these structures were located in the anatomical
167 region where kidneys are expected to form.

168

169 ## *Foxd1*-driven Wt1 loss disrupts ureteric bud branching and cortical organization

170 We used the *Foxd1*^{GC} driver (Kobayashi *et al.*, 2014) to delete *Wt1* specifically in FOXD1^{+} stromal
171 progenitors (Fig. 2A). The FOXD1^{+} stromal progenitors originate from the uncondensed
172 mesenchyme and are first present around E11.0, when they begin populating the cortical and
173 medullary interstitium, the fibrocytes of the capsular tissue and the vascular-supporting
174 pericytes (Kobayashi *et al.*, 2014).

175 Lineage tracing of *Foxd1*^{GC} through tdTomato expression in *ex vivo* control kidney organ
176 cultures confirmed expression in the stromal lineage surrounding the nephrogenic caps and
177 branched ureteric bud (Fig. 2B, left panel; supplementary movie 2A). In contrast, *ex vivo* organ
178 cultures of *Foxd1*^{GC} driven *Wt1*-mutant kidneys showed altered ureteric bud morphogenesis,
179 characterized by reduced branching complexity, elongated and sparser branches, increased
180 spacing between them, and fewer terminal tips (Fig. 2B-C; supplementary movie 2B) - a
181 phenotype similar to that described previously (Weiss *et al.*, 2020). Mutant kidneys are smaller,
182 consistent with reduced branching complexity and fewer nephrogenic caps (Fig. 2D).

183 Histological analysis of E12.5 sections confirmed decreased ureteric bud branching in
184 the *Wt1*-mutants (Fig. 2E). Ureteric bud tips were surrounded by loosely organized NPCs. The
185 *Foxd1*-lineage confirmed strong contribution to the stromal compartment (Fig. 2F, upper panels).
186 We observed some SIX2^{+}tdTomato^{+} cells in the cap mesenchyme of control kidneys (Fig. 2F,

187 white arrows), though these cells expressed lower SIX2 levels compared to surrounding cap
188 mesenchymal. Such double-positive cells were absent in *Foxd1*-driven *Wt1*-mutant kidneys.
189 Staining verified loss of WT1 in the stroma surrounding the cap mesenchyme, while the cap
190 mesenchyme itself remained WT1^{+} (Fig 2F lower panels).

191 At E18.5, mutant kidneys appeared smaller, with expanded cortical stroma between the
192 developing nephrons – consistent with the phenotype described by Weiss et al (Fig. 2G). We
193 observed disrupted nephrogenic zone organization, including SIX2^{+} caps that lost their apical
194 orientation and started moving inwards (Fig. 2H upper panels, white filled arrow; Sup. Fig. S1).
195 This may be the consequence of expansion and migration of cortical stromal cells into the
196 nephrogenic zone. We detected tdTomato^{+} cells in or around proximal tubules (LTL^{+}) (Fig. 2H,
197 white open arrows). It is not clear if these cells are part of the proximal tubules. Staining for WT1
198 in control kidneys at E18.5 showed low expression in the stroma, which was absent in mutants
199 (Fig. 2H lower panels). Proliferative marker KI67 is highly expressed in the nephrogenic zone,
200 comparable to the control kidneys (Sup. Fig. 5A-B).

201

202 Combined nephrogenic and stromal Wt1 loss delays kidney development and initiates
203 blastemal features

204 Targeting the nephrogenic lineage alone caused a severe developmental block, whereas
205 targeting the stromal lineage led to stromal overgrowth, nephrogenic delay, and altered ureteric
206 bud morphogenesis, but each was different form the *Nes*-Cre driven *Wt1* knockout (Berry *et al.*,
207 2015). Since *Wt1* is expressed in both lineages we combined the conditional *Wt1* knockout and
208 tdTomato reporter alleles with the *Wt1*^{CE} knock-in driver (Zhou *et al.*, 2008). The latter is itself a
209 *Wt1*-inactivating allele, so in the tamoxifen induced embryos the Cre-induced loss of the
210 conditional *Wt1* copy results in complete loss of the protein (Fig. 3A). To determine the best
211 window and dosage for targeting the SIX2^{+} nephrogenic lineage and surrounding stroma, we

212 tested single dose Tamoxifen (Tx) injections at E8.5, E9.5, E10.5 or E11.5, on embryonic reporter
213 kidneys isolated at E12.5 and *ex vivo* cultured the kidneys from the treated litters for 48-72hrs.
214 The tdTomato signal indicated the lineage of cells where recombination happened (Fig. 3B).
215 Single Tx injections targeted most of the cells of both lineages when injected at E9.5 or E10.5.
216 Double injections at E9.5 and E10.5 increased this number of targeted cells in the nephrogenic
217 zone. Immunostaining for SIX2 expression showed some cells that lacked tdTomato expression,
218 indicating incomplete Cre activity (Fig. 3B, white arrows). This observation of "escaping"-cells is
219 similar to what has been described for the *Nes*-Cre driven *Wt1* conditional knockout model (Berry
220 *et al.*, 2015) although in this case it is likely due to incomplete activation of the recombinase by
221 tamoxifen.

222 We used the double E9.5+E10.5 Tx treatment to knockout *Wt1*. We compared mutant
223 organs to littermate controls which lacked the CreERT2 allele, but were equally exposed to Tx. In
224 this case the control samples lack Cre activity and will therefore not activate the tdTomato Cre
225 reporter. Lineage tracing of *Wt1*-mutant kidneys revealed smaller kidneys with altered ureteric
226 bud branching and fewer nephrogenic caps (Fig. 3C; supplementary movie 3A-B), similar to the
227 *Foxd1*^{GC} driven mutants. The morphology of the cells suggested that mutant cap mesenchymes
228 lacked epithelialization (Fig. 3C, white arrows), a sign of delayed or blocked MET, a process in
229 which we showed WT1 plays a key role before (Berry *et al.*, 2015; Davies et al., 2004; Essafi *et al.*,
230 2011).

231 Histological assessment at E12.5 showed a thinner NPC layer in mutants compared to
232 controls (Fig. 3D). The NPC population is dispersed, lacking the tight cap-like structure around
233 the ureteric bud tips. The ureteric bud epithelium appears less branched compared to the
234 control. The stroma in the control is relatively thin and confined around the nephrogenic zone,
235 where in the mutant it appears to be expanded – more stroma surrounding the ureteric bud tips
236 and nephron progenitors. The stroma is less organized and seems loosely packed.

237 Immunohistochemistry for SIX2 and tdTomato confirmed incomplete Cre activation in mutants,
238 evidenced by SIX2^{+} tdTomato^{-} cells (Fig. 3E, white arrows), while controls lacked CreERT2 and
239 were tdTomato^{-} (data not shown). Co-staining for SIX2 and WT1 revealed double-positive cells,
240 the "escaping" SIX2^{+} tdTomato^{-} cells (Fig. 3E lower panels). CDH1 staining further supported the
241 presence of widened, misshaped epithelium (Fig. 3E lower panels).

242 Mutant kidneys at E18.5 were markedly smaller, lacked clear corticomedullary
243 segmentation, and displayed severely altered nephrogenesis, with only a few glomeruli present
244 (Fig. 3F). Embryonic-like epithelium was observed in the nephrogenic zone, with emerging
245 blastemal-like regions (Fig. 3F). Staining for proliferative mark KI67 reveals disorganized
246 expression of the protein, with high expression observed in the cortical-region (Sup. Fig. 5B white
247 arrows). Stromal overgrowth was also evident. WT1 immunohistochemistry revealed "escaping"
248 nephrons (Fig. 3G), consistent with observations at E12.5. Mutant kidneys displayed reduced
249 LTL^{+} proximal tubules, consistent with impairment of MET and blocked or delayed nephron
250 differentiation (Fig. 3G).

251

252 ALDH1A2 is the primary contributor to ALDEFLUOR activity in Wilms tumour CSCs

253 Wilms tumor blastema is associated with the Wilms tumor Cancer Stem Cells (CSCs). As
254 mentioned above, the two sets of Wilms tumor CSC markers (NCAM1^{+} with ALDEFLUOR-
255 activity(Pode-Shakked *et al.*, 2013), and SIX2^{+}CITED1^{+}(Murphy et al., 2012; Petrosyan *et al.*,
256 2023)) are both linked to tumor maintenance and progression. In the first marker set, ALDH
257 activity was measured using the ALDEFLUOR assay, which requires living cells, analyzed through
258 flow cytometry. To investigate whether similar NCAM1/ALDH patterns occur during kidney
259 development, we repeated the NCAM1/ALDERED assay (analogous to ALDEFLUOR) on
260 embryonic mouse kidneys. No significant differences were observed between mutant and
261 control kidneys for all lineage-specific *Wt1* mutant kidneys (Sup. Fig. 2).

262 To visualize the protein expression levels of the CSC markers over the course of
263 embryonic kidney development, it was first necessary to determine which ALDH-paralogue was
264 the primary contributor to the ALDEFLUOR assay in WT patient samples. ALDH1A1, ALDH1A2,
265 ALDH1A3 and ALDH2 can all contribute to the detected signal (Zhou *et al.*, 2019). In the context
266 of Wilms tumor, ALDH1A2 has been suggested to be the paralogue associated with CSCs
267 (Petrosyan *et al.*, 2023; Wegert et al., 2020), but its specificity for Wilms tumors has not yet been
268 proven. We reanalyzed microarray data (Shukrun et al., 2014) from Wilms tumor xenograft
269 fractions unsorted and sorted for NCAM1^{+}ALDEFLUOR^{+} and NCAM1^{+}ALDEFLUOR^{-} (Sup. Fig. 3A).
270 The NCAM1+/ALDEFLUOR+ fraction shows high expression for both *ALDH1A2* and *ALDH1A3*.
271 Nonetheless, *ALDH1A3* expression is not enriched in the CSC fraction given its higher expression
272 in the unsorted fraction. *ALDH1A1* is low in all fractions and *ALDH2* is high in unsorted and
273 decreased in both sorted fractions. *ALDH1A2* is the only paralogue specifically upregulated in
274 the NCAM1+/ALDEFLUOR+ faction and therefore these results indicate that ALDH1A2 is the
275 principal contributor to the ALDEFLUOR activity in these Wilms tumor CSCs.

276 To examine ALDH1A-paralogue expression in the developing mouse kidney, E12.5
277 embryonic kidneys were cultured *ex vivo* for 24, 48 and 72 hours and stained for ALDH1A1,
278 ALDH1A2, and ALDH1A3. ALDH1A1and ALDH1A3 were weakly detected in the ureteric bud
279 epithelium, whereas ALDH1A2 showed strong expression in the cortical region of the kidney, in
280 close proximity of the nephrogenic caps, presumably marking stromal cells (Sup. Fig. 3B). Only
281 in the E12.5 kidneys cultured for 48hrs weak ALDH1A2 expression was observed in renal vesicle-
282 shaped structures. Co-staining with FOXD1 antibodies confirmed the stromal identity of the
283 ALDH1A2 positive cells. These findings support ALDH1A2 is mainly localized to the cortical
284 stroma, with weaker protein expression patterns in the epithelializing nephron (Sup. Fig. 3C).

285

286 ## CSC Marker sets for committed and uncommitted NPCs

287 The CSC marker sets were identified on xenograft derived tumor tissues (Petrosyan *et al.*, 2023;
288 Pode-Shakked *et al.*, 2013), which might not reflect the developmental stage of origin anymore.
289 To map these CSC markers onto normal developing kidneys and examine their dynamics in the
290 context of Wilms tumor mutations, we performed immunohistochemistry for NCAM1, ALDH1A2,
291 SIX2, and CITED1 in embryonic kidneys from control and *Wt1*-mutants at E12.5 and E18.5. Due
292 to overlapping antibody host species, ALDH1A2 and CITED1 were analyzed on consecutive
293 sections, resulting in two staining combinations: (NCAM1, ALDH1A2, SIX2; and NCAM1, CITED1,
294 SIX2.

295 In normal embryonic kidneys, NCAM1^{+}ALDH1A2^{+}SIX2^{+} triple-positive cells localized to
296 the SIX2^{+}CITED1^{-} committed NPC/PTA population (Fig. 4A, upper panels, white arrows). These
297 committed NPC/PTA cells exhibited low ALDH1A2 expression compared to surrounding stromal
298 cells. In contrast, the uninduced SIX2^{+}CITED1^{+} cells co-express NCAM1, while they lack
299 ALDH1A2 expression, defining a more uninduced NCAM1^{+}CITED1^{+}SIX2^{+} population (Fig. 4 A,
300 lower panels). Therefore, in normal developing kidneys ALDH1A2 and CITED1 display a mutually
301 exclusive expression pattern. Early nephron structures such as comma- and S-shaped bodies
302 strongly expressed NCAM1 and ALDH1A2 but lacked SIX2 and CITED1, consistent with
303 expression patterns in other studies(Li *et al.*, 2020; Li *et al.*, 2017; Markovic-Lipkovski *et al.*,
304 2007).

305 Lineage-specific *Wt1* loss revealed distinct effects on these populations. *Six2*^{GCiP}-driven
306 *Wt1* mutants at E12.5 showed a reduction in NCAM1, CITED1, and SIX2 expression, while
307 ALDH1A2 expression was observed in the same region where *Wt1* was lost (Fig. 4B upper panels,
308 Fig. 2E). This suggests that *Wt1*-deficient cells obtained an alternative identity, possibly
309 differentiating towards stroma which is characterized by ALDH1A2 expression but not the other
310 markers. At E18.5, the kidney remnants showed a distinct expression pattern as observed at

311 E12.5. The kidney remnant represents a homogenous tissue structure where NCAM1 is
312 expressed, ALDH1A2 is high in the nucleus, SIX2 is low and CITED1 is lowly expressed in the
313 nucleus (Fig. 4B, lower panels). *Foxd1*^{GC} driven *Wt1* mutants resembled controls, without
314 changed CSC marker expression at E12.5 (Fig. 4C). However, we do observe a decline in
315 ALDH1A2 expression at E18.5 (Fig. 4C). In the *Wt1*^{CE} model, at E12.5, NCAM1^{+}ALDH1A2^{+}SIX2^{+}
316 triple-positive cells localized to the committed NPCs/PTA similar to controls (Fig. 4D upper
317 panel). By E18.5, ALDH1A2^{+} regions expanded substantially, likely reflecting increased stromal
318 content, whereas NCAM1^{+}ALDH1A2^{+}SIX2^{+} triple-positive committed NPCs/PTA were scarce,
319 consistent with impaired MET (Fig. 4D). The NCAM1^{+}CITED1^{+}SIX2^{+} uninduced NPC population
320 was present at E12.5, with CITED1 also observed in the committed NPCs/PTA (Fig. 4D lower
321 panels, white arrow), demonstrating CITED1 retention beyond the uncommitted NPC stage. We
322 cannot test directly if these triple-positive committed NPCs/PTA co-express ALDH1A2 due to the
323 overlapping antibody species, but ALDH1A2 expression in similar structures was observed (Fig.
324 4D upper panels). By E18.5, the disorganized nephrogenic zone co-expressed
325 NCAM1^{+}CITED1^{+}SIX2^{+} in the caps, in line with observations in the control kidneys (Fig. 4.D lower
326 panel) representing ALDH1A2^{-} uninduced NPCs.
327

328 LIN28B-overexpression induces developmental disorganization and early Wilms tumor
329 blastema

330 To compare the lineage-specific *Wt1* loss phenotype and WT CSC marker behavior to other
331 Wilms tumor mutations, we examined the effects of LIN28B overexpression on kidney
332 development using the doxycycline (dox)-inducible model (Urbach et al., 2014). We used the
333 same *Wt1*^{GC} driver used by Urbach et al. to control lineage-specificity of the model, but added an
334 additional *lgs7*$^{TRE\text{-LSL-tdTomato}}$ allele (Madisen et al., 2015) to express a tdTomato reporter to identify
335 lineage-specific dox-induced cells (Fig. 5A). Doxycycline was provided from beginning of
336 gestation (E0). *Ex vivo* kidney organ cultures of control littermates lacked the *Wt1*^{GC} allele but

337 were exposed to doxycycline throughout gestation and *ex vivo* culturing, and showed a normally
338 developing embryonic kidney without the reporter because of the lack of the Cre allele (Fig. 5B,
339 upper panel; supplementary movie 4A). Lineage tracing of the mutant kidneys in organ cultures
340 confirmed dox induced tdTomato expression, thus LIN28B overexpression, in the three lineages
341 of the developing kidney (Fig. 5B, lower panels). The tdTomato signal was particularly strong in
342 the ureteric bud, while to lesser extend in the nephrogenic and stromal cells. Mutant kidneys in
343 organ cultures exhibited enlarged nephrogenic caps and delayed epithelialization based on the
344 morphology of the cells, identified at E12.5 + 72 hours of kidney culture (Fig. 5B; supplementary
345 movie 4B).

346 Histological analysis of LIN28B mutants at E12.5 showed the first signs of delayed
347 nephrogenesis with fewer renal vesicle-like structures and disorganized epithelium, and
348 increased stroma between the caps (Fig. 5C, left panel). By E18.5, mutant kidneys displayed
349 disorganized caps and surface indentations (Fig. 5C, right panel, orange arrows). The mutant
350 kidney exhibited regions where normal nephrogenesis occurred, alternated with blastemal-like
351 regions (Fig. 5C, red arrows and circles). These blastemal-like regions surrounding a tubular
352 $CDH1^{+}$ structure are possibly NPCs surrounding a ureteric bud tip that turned inwards, possibly
353 explaining the observed indentations. Staining for SIX2 expression revealed that surface
354 indentations are lined by $SIX2^{+}$ caps turning inwards (Fig. 5D, lower panel). Morphologically this
355 is suggestive for lobe formation, a phenomenon observed in human kidney development but not
356 in mice. At E12.5, WT1 expression is low in the mutant compared to control. While at E18.5 the
357 expression pattern is similar to control, but the caps are enlarged (Fig. 5D).

358 The lobes observed at E18.5 were lost by postnatal day 19 (P19). At P19, the cortico-
359 medullary segmentation disappeared, and the abnormalities in mutant kidneys developed into
360 regions where immature embryonal-appearing epithelium was accompanied by small areas of
361 blastema and stroma, potentially representing beginning Wilms tumors (Fig. 5E). These

362 blastemal-like regions co-expressed SIX2 and WT1, surrounding CDH1^{+} embryonal-appearing
363 epithelium, possibly resembling embryonic cap mesenchymes (Fig. 5F). The SIX2^{+} blastemal-like
364 regions exhibited expression patterns similar to committed NPCs, with gradual decline of SIX2
365 expression while WT1 remained robustly expressed (Fig. 5F, white arrows). The regions that lost
366 SIX2 appeared to be capable of progressing into RV-like shapes (Fig. 5F, orange arrows).

367

368 ## LIN28B-overexpression preserves embryonic marker profiles postnatally

369 We repeated the NCAM1/ALDERED assay on embryonic kidneys from the LIN28 model, but again
370 no significant differences were observed between mutant and control kidneys (Sup. Fig. 4).
371 Visualization of the four CSC protein markers revealed that the NCAM1^{+}ALDH1A2^{+}SIX2^{+}
372 committed NPCs/PTA were absent in the mutant kidneys at E12.5, consistent with delayed
373 nephrogenesis (Fig 6A upper panels). NCAM1^{+}ALDH1A2^{+} epithelialized structures, similar to
374 RV/comma- and S-shaped bodies, lacked SIX2 expression (Fig. 6A, white arrows). We observed
375 NCAM1^{+}CITED1^{+}SIX2^{+} committed NPCs/RVs (Fig. 6A lower panels, white arrows), similar as
376 described for the *Wt1*^{CE} *Wt1* mutant kidneys. By E18.5, NCAM1^{+}ALDH1A2^{+}SIX2^{+} triple-positive
377 cells were detected within the nephrogenic zone in close proximity to the indentations (Fig. 6B,
378 upper panel, white arrow). Their expression pattern resembles committed NPCs/PTA, but their
379 spatial localization differed from that of canonical NPCs/PTAs within the nephrogenic niche. The
380 observed positioning implies that these cells may have been captured in a state, potentially
381 representing the earliest stages of blastema formation, rather than undergo nephron
382 differentiation. This same blastemal-like population of cells co-expressed NCAM1^{+}CITED1^{+}SIX2^{+}
383 in consecutive sections, suggesting all four CSC makers are co-expressed in the same cells in
384 this early blastemal-like population (Fig. 6B lower panels, white arrows).

385 By P19, blastemal regions which we previously showed were positive for SIX2 and WT1
386 (Fig. 5F) exhibited robust expression of NCAM1, ALDH1A2, CITED1, and SIX2, shown on

consecutive sections (Fig. 6C). Co-staining of consecutive sections demonstrated specific expression patterns for ALDH1A2 and CITED1, with differential expression patterns for each in distinct parts of the blastema (Fig. 6C, green arrow: high ALDH1A2, orange arrow: high CITED1, asterisk: both proteins expressed). This suggests that the blastemal-like population is a heterogenous population of cells, possibly reflecting uninduced NPC state when CITED1^{high}ALDH1A2^{low}, and induced NPC state when CITED1^{low}ALDH1A2^{high}. We found a third population which is quadruple-positive for all markers (Fig. 6C asterisks), and this could represent a transitional state between uninduced and induced blastema, which is only present in the mutant. Blastemal populations surrounded embryonic-like tubular structures, potentially remnants of UB tips. This is similar to the phenotype described by Urbach et al. (2014), who claim that these blastema structures are remains of cap mesenchymes, and that these structures are capable of differentiating into nephrogenic structures in the presence of *Wnt4* (Urbach *et al.*, 2014). These blastemal cells remained proliferative, as evidenced by KI67 expression (Sup. Fig. 5).

402 ## Methods

403

404 ### Animals

405 The animal care and experimental procedures were approved by the Animal Welfare Body Leiden
406 and are in accordance with the Dutch Experiments on Animals Act and EU Directive 2010/63/EU.
407 For timed pregnancies, males Wt1$^{tm2(cre/ERT2)Wtp}$/J, Wt1$^{tm1.2Ndha}$Six2$^{tm1(EGFP/cre)Phoh}$ and
408 Wt1$^{tm1.2Ndha}$B6;129S4-Foxd1$^{tm1(GFP/Cre)Amc}$/J were crossed with female Wt1$^{tm1.1Ndha}$ to conditionally
409 knockout Wt1. To activate the CreERT2 in the WT2 mouse, tamoxifen (Sigma: T5648) (2mg/40g
410 body weight) dissolved in corn oil (Sigma: C8267) was administered intraperitoneally. Pregnant
411 females received injections at E8.5, E9.5, E10.5, E11.5, or combined at E9.5 and E10.5. To
412 conditionally activate LIN28B, male Wt1$^{tm1(EGFP/cre)Wtp}$/J and Wt1$^{tm1(EGFP/cre)Wtp}$/J*B6.Cg-Igs7$^{tm62.1(tetO-}$
413 $^{tdTomato)Hze}$/J were crossed with female B6.Cg-Gt(ROSA)26Sor$^{tm1(rtTA*M2)Jae}$B6.Cg-Col1a1$^{tm2(tetO-}$
414 $^{LIN28B)Gqda}$. Doxycycline (Thermo Fisher Scientific, 24390-14-5) (1g/L) was provided via the drinking
415 water to the pregnant female mouse at E0. Pregnant females were euthanized by cervical
416 dislocation for collection of (embryonic) kidneys. Pups at P19 were euthanized by cervical
417 dislocation for kidney collection.

418

419 ### Ex vivo kidney organ culture

420 Embryonic kidneys were isolated from E12.5 embryos derived from the mouse model crosses
421 described above. Kidneys were dissected and placed on a Transwell polyester membrane insert
422 (0.4 µm pore size, Corning, 3450) in six-well plates. The lower chamber was filled with 1ml kidney
423 culture medium to establish an air-liquid interface. The culture medium consisted of DMEM
424 [Gibco 41966029], MEM Non-Essential Amino Acids 1x [Gibco 11140035], Penicillin-
425 Streptomycin 5U/ml [Gibco 15070063], βMeOH 50µM [Gibco 31350010] and 10% FCS, with or
426 without doxycycline (2µg/mL). Cultures were maintained at 37°C in 5% CO_2. After 1hr, when

427 kidneys had attached to the membrane, imaging was started in an on-stage incubator chamber.
428 Images were acquired every hour for 72-96 h. When finished, kidneys were fixed in 4%
429 paraformaldehyde (PFA) in 1xPBS for 20', washed 3x10' in 1xPBS, followed by whole kidney
430 immunofluorescent staining as described below.
431

432 Histological and immunofluorescent staining

433 Freshly isolated (embryonic) kidneys or whole embryos were fixed in 4% PFA and embedded in
434 paraffin. Smaller tissues were first embedded in 2% low-melting agarose prior to paraffin
435 embedding. 5 µm sections were made using a microtome. Slides with sections were dewaxed
436 with xylene and rehydrated through a series of washes with 100%, 95% and 80% ethanol.
437 Hematoxylin (Agilent, S330930-2) staining was performed through the following protocol: slides
438 were rinsed in deionized water, followed by 3' in hematoxylin, rinsed in deionized water, 5' under
439 running tap water, 12x dipped in acid ethanol, 2x1' in tap water, 1x2' in deionized water. For the
440 eosin (Sigma-aldrich, HT110232) stain, slides were stained for 30" in eosin solution, followed by
441 1' in 80% ethanol, 1' in 90% ethanol, 1' in 100% ethanol and 2x5' in xylene before being mounted
442 with Pertex (Histolab, 00811-EX). For immunofluorescent staining, antigen retrieval was
443 performed in 10mM sodium citrate (J.T.Baker, 6132043) buffer with 0.05% Tween-20 (Sigma
444 Aldrich, 274348) (pH 6.0) in a pressure cooker for 20'. Slides were blocked in 1x PBS with 2%
445 serum for 1hr at RT. Primary antibodies were incubated o/n at 4°C, followed by washing 3x10' in
446 1xPBS the next day. Secondary antibodies were incubated o/n at 4°C, followed by co-staining for
447 DAPI (Polysciences, 09224-10) and mounting with FluorSave reagent (Merck Millipore, 345789).
448 Primary antibodies: Wt1 (1:50; Abcam, ab89901), Six2 (1:200; Abnova, H00010736-M01), E-
449 cadherin/Cdh1 (1:200; BD Biosciences, 610182), Ncam1 (1:40; R&D systems (Bio Techne),
450 AF2408), Aldh1a2 (1:100; Abcam, ab96060), Cited1 (1:200; ThermoFisher, 26999-1-AP), LTL
451 unconjugated-biotinylated (1:400; Vector laboratories, L-1320-5), tdTomato (1:100;
452 ThermoFisher, TA150128), Ki-67 (1:200; ThermoFisher, MA5-14520). Secondary antibodies: Goat

anti-Rabbit IgG Cross-Adsorbed Secondary Antibody, Alexa Fluor 647 (1:1000; Thermofisher, A32733), Goat anti-Mouse IgG1 Cross-Adsorbed Secondary Antibody, Alexa Fluor 488 (1:1000; Thermofisher, A21121), Goat anti-Mouse IgG2a Cross-Adsorbed Secondary Antibody, Alexa Fluor 568 (1:1000; Thermofisher, A21134), Streptavidin, Alexa Fluor 546 conjugate (1:1000; Thermofisher, S11225), Donkey Anti-Goat IgG H&L (Alexa Fluor® 405) preadsorbed (1:1000; Abcam, ab175665), Donkey Anti-Rabbit IgG (H+L) Cross-adsorbed, Alexa Fluor 647 (1:1000; Thermofisher, A31573), Donkey Anti-Mouse IgG (H+L) Highly Cross-Adsorbed, Alexa Fluor 488 (1:1000; Thermofisher, A21202).

Additional methods can be found in the supplementary files.

465 ## Discussion

466 Due to the early embryonic origin of Wilms tumors, little is known about the earliest phenotypic
467 changes following tumor-initiating mutations. Genetically engineered mouse models provide a
468 unique and powerful model to study these effects in a controlled and well-understood
469 developmental context. Here we present an extensive characterization of the early events after
470 Wilms tumor mutation induction in mouse models.

471 Previous studies in human Wilms tumor xenografts identified two marker sets for CSCs:
472 NCAM1^{+} with ALDEFLUOR-activity (Pode-Shakked *et al.*, 2013) and SIX2^{+}CITED1^{+}(Murphy *et al.*,
473 2012; Petrosyan *et al.*, 2023). We identified that NCAM1^{+}ALDH1A2^{+} cells (ALDH1A2 as the
474 paralogue representative for the ALDH-activity in the xenograft derived CSCs) are present in
475 normal embryonic kidneys, specifically in nephron progenitor cells/pretubular aggregates
476 (NPC/PTA) and early nephron structures (comma- and S-shaped bodies) stages (Fig. 7A). Their
477 presence in *Wt1* mutants reflects disrupted nephrogenesis rather than tumor-specific
478 expression, supporting the idea that CSC markers are retained or co-opted from developmental
479 hierarchies. The mutual exclusivity of CITED1 and ALDH1A2 expression in normal embryonic
480 kidneys defines cells with CITED1^{+} marking uninduced NPCs and ALDH1A2^{+} cells marking
481 committed NPCs.

482

483 ### *Lineage specific Wt1-loss results in lineage confusion*

484 Loss of *Wt1* driven by *Six2*^{GCiP} keeps mutant cells in mesenchymal cell state, or shifts the cells to
485 an even more mesenchymal character, as supported by the migration of mutant cells in our
486 timelapse data. WT1 controls the mesenchymal to epithelial transition in kidney cells (Essafi *et*
487 *al.*, 2011), therefore loss of *Wt1* at this stage could lead to a block in MET or even reversal to
488 earlier stages. Mutant cells lost SIX2 and NCAM1, while ALDH1A2 was present. This is consistent
489 with *in vitro* evidence that WT1 represses ALDH1A2 (Li *et al.*, 2017). An NCAM1^{-}ALDH1A2^{+}SIX2^{-}

490 state is not a canonical feature of normal early nephron development, although ALDH1A2
491 expression on its own is a hallmark for cortical stromal cells. This could suggest that loss of *Wt1*
492 in NPCs causes a lineage-shift towards a stromal fate (Fig. 7B). A precedent for this is the NPC-
493 specific knockout of *Pax2* (Naiman et al., 2017). However, the loss of many markers that are
494 informative for kidney development by the E18.5 timepoint prevents us from drawing firm
495 conclusions here, and an even greater developmental diversion to pre-renal or non-renal cell
496 types cannot be excluded. We identified altered CSC marker expression. NCAM1 is expressed,
497 and ALDH1A2 and CITED1 localize to the nucleus. This latter one is observed in primitive
498 blastema, which might play a role in Wilms tumor pathogenesis (Lovvorn et al., 2007). Predicted
499 postnatal lethality prevents analysis of postnatal stages of this mutant model.

500 The *Foxd1*^{GC}-driven *Wt1* loss closely resembles the previously published phenotype
501 (Weiss *et al.*, 2020) Mutant kidneys are smaller with disrupted nephrogenic zones, expanded
502 stroma, and delayed UB branching (Fig. 7C). The UB branching defects have previously been
503 linked to reduced retinoic acid signaling and therefore reduced ALDH1A2 expression in the
504 stroma in the *Foxd1*^{GC} driven *Wt1*-mutant kidneys (Weiss *et al.*, 2020). We observed a stromal
505 reduction of ALDH1A2 expression in the *Foxd1*^{GC} mutant at E18.5, but not at E12.5. This could
506 indicate only partial dependence of ALDH1A2 expression on *Wt1* in the stroma, which may
507 explain why Weiss and colleagues only partly rescued the phenotype through retinoic acid
508 supplementation (Weiss *et al.*, 2020). We found SIX2^{+} caps were occasionally displaced inward,
509 raising the possibility of aberrant lobulation (see below). Through lineage tracing of the stromal
510 population we identified SIX2^{+} tdTomato^{+} cells in the cap mesenchyme of control kidneys (Fig.
511 2F, white arrows), though these cells expressed lower SIX2 levels compared to surrounding cap
512 mesenchyme. This could confirm a previously suggested small contribution of the *Foxd1*-lineage
513 to the *Six2*-expressing cells (Kobayashi *et al.*, 2014). The nephrogenic and stromal lineages are
514 believed to share a common *Osr1*$^{+}$ mesenchymal progenitor prior to lineage segregation
515 (Mugford et al., 2008). Transcriptomic data from *WT1*-mutant Wilms tumor cell lines supports

516 this developmental connection (Royer-Pokora et al., 2023). In these tumor cells, co-expression
517 of FOXD1 and SIX2 was observed, a pattern also found in human NPCs (Lindstrom et al., 2018a).
518 The existence of such a co-expressing population in normal development could imply that spatial
519 or signaling cues determine whether cells adopt SIX2^{+} nephron progenitor or FOXD1^{+} stromal
520 fates. The minor *Foxd1*-lineage contribution to the SIX2^{+} cap mesenchyme could then reflect
521 residual plasticity of this early progenitor pool. Following *Wt1* loss, the observed reduction of
522 *Foxd1*-lineage contribution to SIX2^{+} population may indicate premature lineage restriction or
523 altered mesenchymal identity. Lack of blastemal development in the *Foxd1*^{GC} driven Wt1
524 mutants could imply that in contrast to *Six2* (Kobayashi *et al.*, 2014), *Foxd1* is not a direct target
525 of *Wt1*.

526 *Wt1*^{CE}-induced *Wt1* loss in most nephrogenic and stromal cells and revealed blastemal-
527 like populations by E18.5 and showed "escaping" nephrons adjacent to mutant zones. The
528 escaping nephrons are likely the result of the incomplete activation of Cre through tamoxifen
529 induction, leaving a mosaic pattern of activated and incompletely activated cells next to each
530 other. This mosaic model provides an unique opportunity to study cell–cell interactions, since
531 wildtype and mutant cells coexist. This milder phenotype, compared to the severely altered
532 *Six2*^{GC} *Wt1* mutants, suggests that the timing and mosaic nature of recombination modulate
533 disease severity. Mutants NPCs could be partially by remaining wildtype NPCs. Disruption of
534 NPCs may alter signaling to the stromal cells (which have also lost *Wt1* themselves), with both
535 disturbed lineages contributing to Wilms tumor development. Alternative, in this model we target
536 the OSR1^{+} progenitor cells, suggesting that the timing of mutation plays an important role rather
537 than the specific lineage. In this model we observed committed NPCs/PTA co-expressing the four
538 CSC makers, while at E18.5 most of these induced structures were lost due to proposed blocked
539 MET. Mutant cells either possess the plasticity to shift between committed and uncommitted
540 stages, or alternatively there is a lineage shift towards stroma, leading to a stromal phenotype
541 and increased ALDH1A2 (Fig. 7D).

542 This *Wt1*^{CE}-driven model further shows the complexities of temporal specificity
543 (developmental stage) and spatial specificity (lineage) during kidney development. Our lineage
544 tracing data show that our tamoxifen regiment targets both nephrogenic and stromal lineage, but
545 at present we cannot distinguish between targeting both lineages at the same time, or targeting
546 a common precursor state of these two lineages. This is an important distinction for the definitive
547 interpretation of the data, and additional Cre drivers would be required to answer this question.
548 However better understanding of the developmental steps leading to the formation of the early
549 metanephros is essential to identify candidates for this.

550

551 *LIN28B Overexpression blocks cells in an embryonic state*

552 *LIN28B* overexpression produced a distinct but complementary phenotype compared to *Wt1*
553 loss. Kidneys displayed enlarged nephrogenic caps, embryonic lobulation-like features, and
554 disrupted corticomedullary organization (Fig. 7E).

555 The persistence of embryonic-like ureteric bud tips surrounded by NPCs in adult kidneys
556 raises the possibility that the presence of NPCs maintains ureteric bud tips in an
557 undifferentiated, "early" state, preventing their maturation into collecting duct epithelium.
558 Although speculative, there are strong reciprocal cell-cell interactions between the ureteric bud
559 and metanephric mesenchyme. In normal kidney development, metanephric mesenchyme
560 produces GDNF, which binds the Ret receptor on the ureteric bud cells. Besides GDNF, other
561 factors like WNT11 and FGF signaling molecules sustain NPC proliferation and self-renewal
562 (Costantini and Kopan, 2010; Grieshammer et al., 2005; Majumdar et al., 2003). Thus, the
563 prolonged presence of NPCs may create a niche environment that stabilizes or delays the
564 ureteric bud tip differentiation into mature collecting duct structures.

565 At P19, the blastemal regions display a gradual decline of SIX2 expression, while WT1
566 remains stable. This patterns is suggestive for MET, similar to NPCs in normal nephron

567 development where the committed NPCs lose SIX2 expression to go through MET, while WT1
568 maintains expressed (Davies *et al.*, 2004; Hastie, 2017; Mugford *et al.*, 2009). While overall SIX2
569 and NCAM1 remain broadly expressed, CITED1 and ALDH1A2 exhibit distinct but partially
570 overlapping domains. We identify cells expressing either CITED1 or ALDH1A2, as well as a small
571 population co-expressing both markers, suggesting the presence of a transitional state between
572 uncommitted and committed state. The differences could be further explained by the fact that
573 LIN28B represses let-7 maturation, supporting maintenance of stem cell properties of the
574 blastemal population. Therefore, CITED1 remains expressed and ALDH1A2 repressed, keeping
575 the potential for differentiation in the progenitors.

576 Together, these observations suggest that LIN28B disrupts the normal temporal coordination
577 between NPCs and ureteric bud tip differentiation, maintaining both compartments in an
578 embryonic-like state. The persistence of lobulation, the presence of transitional
579 CITED1^{+}ALDH1A2^{+} cells, and the maintenance of undifferentiated ureteric bud tips suggests the
580 importance of precise temporal regulation of progenitor exhaustion leading to ureteric bud
581 maturation.

582

583 *Formation of kidney lobules*

584 Two of our models show signs of kidney lobulation. At E18.5, we observed lobulation in the
585 mutant LIN28 kidneys. This observation was specific to E18.5 mutant kidneys and absent in the
586 mutants by P19, when there is no cortical-medullary segmentation anymore and regions with
587 blastema are alternated with normal appearing tubules and glomeruli throughout the whole
588 kidney. In addition, in the *Foxd1*^{GC} *Wt1* model we observed some SIX2^{+} cap mesenchymes
589 displaced inward, which could be a milder version or earlier stage of the phenotype observed in
590 the LIN28 model.

591 The mechanism driving kidney lobulation and the physiological purpose are unknown, but
592 lobulation is normally not a feature of murine kidneys. It is suggested that human lobulation
593 occurs through striated cells, presumably of interstitial origin, that align along the radial axis of
594 the kidney (Lindstrom et al., 2018b). This is consistent with our observation of stromal cells
595 infiltrating the nephrogenic zone, possibly "dragging" these caps to the inner parts of the cortex.
596 Further study on human lobulation is necessary to draw any further conclusions on this
597 observation.

598

599 *Relevance for human Wilms tumors*

600 The data presented here provide an extensive characterization of the early phenotypic events
601 after Wilms tumor initiation at the level of separate cell lineages, at several time points, for two
602 different Wilms tumor genes. *Wt1* loss disrupts lineage commitment and drives mesenchymal
603 persistence, LIN28B overexpression disrupts developmental timing and prevents progenitor
604 differentiation. While both mutations in patients result in Wilms tumor development, the
605 underlying molecular mechanism appears different. Further investigation on the transcriptional
606 and epigenetic mechanisms driving these phenotypes could lead to clarification of the
607 underlying mechanisms. As at present 46 Wilms tumor genes are known in different functional
608 classes (Spreafico *et al.*, 2021), the complexity of Wilms tumor biology might be even greater than
609 presented here for *Wt1* and LIN28 mutations. Care should be taken when generalizing
610 conclusions from studying Wilms tumor cases with different initiating mutations, or cases where
611 these are unknown. Differences in underlying biology for different Wilms tumors could implicate
612 differences in therapeutic potential and impossibilities, and should therefore also be taken into
613 account when designing pre-clinical studies and clinical trials.

614

615 Figure legends

616

617 **Figure 1: *Six2*^{GCiP} driven *Wt1*-mutant model characterization.**

618 (A) Schematic representation of the *Six2*^{GCiP} lineage specific knockout of *Wt1* in the mouse
619 model.
620 (B) *Ex vivo* kidney organ culture of E12.5 control (left) and *Wt1* mutant kidney (right), with
621 eGFP linked to SIX2 expression and TdTomato representing the lineage. Scale 200µm.
622 (C) Staining for SIX2, TdTomato and CDH1 on *ex vivo* kidney organ cultures of a control and
623 *Wt1* mutant kidney. Scale 100µm.
624 (D) H&E staining of control and *Wt1* mutant kidneys at E12.5. Scale 50µm.
625 (E) Staining for TdTomato to validate lineage and WT1 to validate knockout in E12.5 control
626 and mutant kidneys. Scale 100µm.
627 (F) H&E staining of control and *Wt1* mutant kidneys at E18.5. Scale 50µm.
628 (G) Staining for SIX2, CDH1 and WT1 to elucidate identity of E18.5 mutant kidneys. Scale
629 100µm.

630

631 **Figure 2: *Foxd1*^{GC} driven *Wt1*-mutant model characterization**

632 (A) Schematic representation of the *Foxd1*^{GC} lineage specific knockout of *Wt1* in the mouse
633 model.
634 (B) *Ex vivo* kidney organ culture of E12.5 control (left) and *Wt1* mutant kidney (right), with
635 eGFP linked to FOXD1 expression and TdTomato representing the lineage. Scale 200µm.
636 (C) Absolute quantification of the number of cap mesenchymes in the control versus mutant
637 kidney, quantified from the *ex vivo* kidney organ culture.
638 (D) Staining of DAPI and CDH1 on the *ex vivo* kidney culture. Scale 100µm.

639 (E) H&E staining of control and *Wt1* mutant kidneys at E12.5. Scale 50µm.

640 (F) Staining for TdTomato to validate lineage and WT1 to validate knockout in E12.5 control
641 and mutant kidneys. Scale 100µm. White arrowheads indicate Foxd1 lineage
642 contribution to SIX2+ cells.

643 (G) H&E staining of control and *Wt1* mutant kidneys at E18.5. Scale 50µm.

644 (H) Staining for TdTomato to validate lineage and WT1 to validate knockout in E18.5 control
645 and mutant kidneys. Scale 100µm. White open arrows indicate Foxd1-lineage in or
646 around proximal tubules.

647

648 **Figure 3: *Wt1^{CE}* driven *Wt1*-mutant model characterization**

649 (A) Schematic representation of the *Wt1^{CE}* spatial and temporal specific knockout of *Wt1* in
650 the mouse model.

651 (B) Optimization of Tx injection at E8.5, E9.5, E10.5 or E11.5, and double injections at E9.5 +
652 E10.5, analyzed in *ex vivo* kidney cultures at E12. Cells labeled with white arrows are a
653 representation of the tamoxifen treatment escaping cells. White arrowheads indicate
654 cap mesenchyme cells that escaped tamoxifen-induced Cre activation. Scale 60µm.

655 (C) *Ex vivo* kidney organ culture of E12.5 control (upper) and *Wt1* mutant kidney (lower), with
656 TdTomato representing the lineage. White arrows highlight epithelializing structures.
657 White arrowheads indicate epithelialized structures based on morphology of the cells.
658 Scale 200µm.

659 (D) H&E staining of control and *Wt1* mutant kidneys at E12.5. Scale 50µm.

660 (E) Staining for TdTomato to validate lineage and WT1 to validate knockout in E12.5 control
661 and mutant kidneys. White arrowheads indicate cap mesenchyme cells that escaped
662 tamoxifen-induced Cre activation. Scale 100µm.

663 (F) H&E staining of control and *Wt1* mutant kidneys at E18.5. Scale 50µm.

664 (G) Staining for TdTomato to validate lineage and WT1 to validate knockout in E18.5 control
665 and mutant kidneys. LTL marks proximal tubules. White arrows indicate nephrogenic(-
666 derived) WT1 expression indicating the escaped regions. Scale 100µm.

667

668 **Figure 4: Cancer Stem Cell marker expression in lineage-specific *Wt1* mutant kidneys**

669 (A) Staining for CSC markers NCAM1, ALDH1A2, SIX2 and CITED1 in the normal developing
670 embryonic kidney at E12.5 and E18.5. White arrows indicate triple-marker expressing
671 cells. Scale 100µm.
672 (B) CSC marker expression in *Six2*^{GCiP} driven *Wt1* mutant kidneys at E12.5 and E18.5. Scale
673 100µm.
674 (C) CSC marker expression in *Foxd1*^{GC} driven *Wt1* mutant kidneys at E12.5 and E18.5. White
675 arrows indicate triple-marker expressing cells. Scale 100µm.
676 (D) CSC marker expression in *Wt1*^{CE} driven *Wt1* mutant kidneys at E12.5 and E18.5. White
677 arrows indicate triple-marker expressing cells. Scale 100µm.

678

679 **Figure 5: Characterization of the LIN28B overexpression model**

680 (A) Schematic representation of the doxycycline inducible LIN28B overexpression model,
681 with (representing mutants) and without (representing doxycycline exposed control
682 littermates) tdTomato reporter.
683 (B) *Ex vivo* kidney organ culture of E12.5 control (upper) and LIN28B mutant kidney (lower).
684 Scale 200µm.
685 (C) H&E staining of control and LIN28B mutant kidneys at E12.5 (left panel) and E18.5 (right
686 panel). Scale 50µm.
687 (D) Staining for WT1, SIX2 and CDH1 to identify phenotype at E12.5 and E18.5. Scale 100µm.

688 (E) H&E staining of control and LIN28B mutant kidneys at P19. Scale 50µm.

689 (F) Staining for WT1, SIX2 and CDH1 to identify blastemal phenotype at P19. White arrows
690 indicate SIX2+WT1+ cells, orange arrows indicate SIX2-WT1+ cells, hinting towards
691 commitment to the epithelial lineage. Scale 100µm.

692

693 **Figure 6: Cancer Stem Cell marker expression in LIN28B overexpression mutant kidneys**

694 (A) CSC marker expression in E12.5 LIN28B overexpression kidneys. White arrows indicate
695 triple-marker expressing cells. Scale 100µm.

696 (B) CSC marker expression in E18.5 LIN28B overexpression kidneys, showing early
697 blastemal-like cells co-expressing all four markers in the same cells indicated by the
698 white arrows on consecutive sections. Scale 100µm.

699 (C) CSC marker expression in P19 LIN28B overexpression kidneys, showing blastemal-like
700 cells with distinct patterns for ALDH1A2 and CITED1 expression, and a transitional cell
701 co-expressing all four markers in the same cell. High protein expression is indicated with
702 an orange arrow, low protein expression with a green arrow and the transitional cells are
703 indicated with asterisks. Scale 100µm.

704

705 **Figure 7: Schematic representation of genotype-phenotype speculations of Wilms tumor**
706 **driver mutations.**

707 (A) CSC marker expression over the course of nephrogenesis, in the nephrogenic and
708 stromal lineage.

709 (B) *Six2*^{GCiP} driven loss of Wt1 results in severe block of nephrogenesis, and possibly results
710 in lineage confusion based on CSC marker expression.

711 (C) *Foxd1*^{GC} driven Wt1 loss results in expanded stroma and a ureteric bud branching
712 phenotype.
713 (D) Conditional loss of Wt1 through the *Wt1*^{CE} tamoxifen dependent administration results in
714 stromal and ureteric bud phenotype and a mild block of nephrogenesis. Here the first
715 suggestive quadruple-positive CSC markers come together in the same cells possibly
716 giving rise to blastema.
717 (E) LIN28B overexpression results in delayed nephron epithelialization, embryonic lobe
718 formation and blastemal-like cells co-expressing the four CSC markers.
719

720 # Supplementary

721

722 ## Supplementary methods

723 ### *Ncam1/ALDERED assay for flow cytometry*

724 Embryonic kidneys from E12.5 embryos were directly dissociated with Trypsin/EDTA (0.05%)
725 (Gibco, REF25300) for 3' at 37°C. (Embryonic) kidneys from E18.5 and P19 were first minced into
726 small pieces using a scalpel, prior to dissociation. After incubation, tissues were vigorously
727 pipetted up and down to dissociate into single cells. DMEM + 10% FCS was used to inactivate the
728 trypsin. Cells were centrifuged 5' at 300g and resuspended in FACS buffer (PBS + 0.5% BSA +
729 0.04M EDTA). Clumps were removed by using a 35µm cell strainer. A small fraction was taken at
730 this step to calibrate the flow cytometer. The rest of the single cells were stained for Ncam1
731 (1:125; NCAM-1/CD56 Antibody, R&D systems, AF2408) with a Donkey-anti-Goat Alexa Fluor 405
732 (1:1500; Abcam, ab175665), followed by the ALDERED assay kit (EMD Millipore, SCR150)
733 according to the manufacturer's protocol. LSRFortessa flow cytometer (BD Biosciences) was
734 used to measure expression.

735

736 ### *Statistical analysis*

737 Due to variable cytometer settings over time, raw data was normalized to paired littermate
738 controls. The DEAB sample was used as the threshold for ALDERED expression. Normalized
739 expression values were compared between controls and mutants from the same time point and
740 Cre driver. Wt1-mutants: Six2-Cre driven E12.5 ctrl (n=9) vs mutant (n=7), Six2-Cre driven E18.5
741 ctrl (n=10) vs mutant (n=6), Foxd1-Cre driven E12.5 ctrl (n=13) vs mutant (n=4), Foxd1-Cre driven
742 E18.5 ctrl (n=14) vs mutant (n=5), Wt1-CE driven E12.5 ctrl (n=9) vs mutant (n=8), Wt1-CE driven
743 E18.5 ctrl (n=6) vs mutant (n=6)). LIN28B mutants: E12.5 ctrl (n=6) vs mutant (n=6) and E18.5 ctrl

744 (n=6) vs mutant (n=6). Groups were compared using a non-parametric Mann-Whitney U test
745 between groups.
746

747 ## Supplementary Figure legends

748 **Sup. Fig. 1: *Foxd1^{GC}* driven *Wt1* mutant.** SIX2+ caps lost their apical orientation and started
749 moving inwards. Scale 100µm.

750

751 **Sup. Fig. 2: NCAM1+/ALDERED flowcytometry assay on Wt1 mutant embryonic kidneys.**

752 (A) Fraction of NCAM1+/ALDERED double positive cells in developing embryonic kidneys
753 comparing control versus Wt1 mutants from the three lineage-specific Cre-drivers at
754 E12.5 and E18.5. No significant differences observed between groups, using a non-
755 parametric Mann-Whitney U test between groups. P-values indicated.
756 (B) Raw data files from the *Six2^{GCiP}* driven control versus mutant kidneys, using DEAB for
757 setting the cutoff for the ALDH activity measured through ALDERED expression.
758 (C) Raw data files from the *Foxd1^{GC}* driven control versus mutant kidneys, using DEAB for
759 setting the cutoff for the ALDH activity measured through ALDERED expression.
760 (D) Raw data files from the *Wt1^{CE}* driven control versus mutant kidneys, using DEAB for
761 setting the cutoff for the ALDH activity measured through ALDERED expression.

762

763 **Sup. Fig. 3: ALDH paralogue expression in Wilms tumor Xenograft microarray data and in**
764 **developing kidneys**

765 (A) ALDH paralogue enrichment in Wilms tumor Xenograft derived CSCs. A comparison
766 between unsorted and sorted fractions, for NCAM1+/ALDEFLUOR- and
767 NCAM1+/ALDEFLUOR+.

768 (B) ALDH paralogue protein staining in *ex vivo* kidney cultures, cultured for 24, 48 and 72
769 hours. Scale bar: 50µm.
770 (C) FOXD1 and ALDH1A2 protein expression in ex vivo kidney cultures cultured for 96 hours.
771 Scale bar: 50µm.

772

773 **Sup. Fig. 4: NCAM1+/ALDERED flowcytometry assay on LIN28B mutant embryonic kidneys.**

774 (A) Fraction of NCAM1+/ALDERED double positive cells in developing embryonic kidneys
775 comparing control versus LIN28B mutants at E12.5 and E18.5. No significant differences
776 observed between groups, using a non-parametric Mann-Whitney U test between
777 groups.
778 (B) Raw data files from the control versus mutant kidneys at E12.5, using DEAB for setting
779 the cutoff for the ALDH activity measured through ALDERED expression.
780 (C) Raw data files from the control versus mutant kidneys at E18.5, using DEAB for setting
781 the cutoff for the ALDH activity measured through ALDERED expression.

782

783 **Sup. Fig. 5: Proliferative marker expression KI67 in *Wt1* and LIN28B mutant (developing)**
784 **kidneys.**

785 (A) KI67 staining for Wt1 mutant kidneys at E12.5 for lineage-specific Cre drivers. Scale
786 100µm.
787 (B) KI67 staining for Wt1 mutant kidneys at E18.5 for lineage-specific Cre drivers. Scale
788 100µm.
789 (C) KI67 staining for LIN28B mutant kidneys at P19. Scale 100µm.

790

Author contributions

N.S.P. performed and analyzed all experiments. D.K., C.M.B, M.M.L., J.W.C.C., C.W.J.C and D.D.Ö supported in the performed experiments and contributed to the supplementary figures. N.S.P and P.H. designed the experiments. N.S.P. prepared figures. N.S.P., K.S.D. and P.H. wrote the manuscript.

Acknowledgements

We thank all members of the Hohenstein lab for valuable discussions. We thank Jorrit Hos and Orhan Demirbacak for help with animals. The research was supported by KiKa (Children Cancer Free Foundation).

Conflict of interest

The authors declare no competing interests.

803 ## References

804 Armstrong, J.F., Pritchard-Jones, K., Bickmore, W.A., Hastie, N.D., and Bard, J.B. (1993). The
805 expression of the Wilms' tumour gene, WT1, in the developing mammalian embryo. Mech Dev *40*,
806 85-97.
807
808 Beckwith, J.B., Kiviat, N.B., and Bonadio, J.F. (1990). Nephrogenic rests, nephroblastomatosis, and
809 the pathogenesis of Wilms' tumor. Pediatr Pathol *10*, 1-36.
810
811 Berry, R.L., Ozdemir, D.D., Aronow, B., Lindstrom, N.O., Dudnakova, T., Thornburn, A., Perry, P.,
812 Baldock, R., Armit, C., Joshi, A., et al. (2015). Deducing the stage of origin of Wilms' tumours from a
813 developmental series of Wt1-mutant mice. Dis Model Mech *8*, 903-917. 10.1242/dmm.018523.
814
815 Bonnet, D., and Dick, J.E. (1997). Human acute myeloid leukemia is organized as a hierarchy that
816 originates from a primitive hematopoietic cell. Nat Med *3*, 730-737. 10.1038/nm0797-730.
817

818 Costantini, F., and Kopan, R. (2010). Patterning a complex organ: branching morphogenesis and
819 nephron segmentation in kidney development. Dev Cell *18*, 698-712. S1534-5807(10)00207-8 [pii]
820 10.1016/j.devcel.2010.04.008.

821
822 Cotino-Najera, S., Garcia-Villa, E., Cruz-Rosales, S., Gariglio, P., and Diaz-Chavez, J. (2024). The role of
823 Lin28A and Lin28B in cancer beyond Let-7. FEBS letters *598*, 2963-2979. 10.1002/1873-3468.15004.
824

825 Davies, J.A., Ladomery, M., Hohenstein, P., Michael, L., Shafe, A., Spraggon, L., and Hastie, N. (2004).
826 Development of an siRNA-based method for repressing specific genes in renal organ culture and its
827 use to show that the Wt1 tumour suppressor is required for nephron differentiation. Hum Mol
828 Genet *13*, 235-246. 10.1093/hmg/ddh015ddh015 [pii].

829 Dolt, K.S., Lawrence, M.L., Miller-Hodges, E., Slight, J., Thornburn, A., Devenney, P.S., and
830 Hohenstein, P. (2013). A universal vector for high-efficiency multi-fragment recombineering of BACs
831 and knock-in constructs. PLoS One *8*, e62054. 10.1371/journal.pone.0062054.
832

833 Essafi, A., Webb, A., Berry, R.L., Slight, J., Burn, S.F., Spraggon, L., Velecela, V., Martinez-Estrada,
834 O.M., Wiltshire, J.H., Roberts, S.G., et al. (2011). A Wt1-controlled chromatin switching mechanism
835 underpins tissue-specific Wnt4 activation and repression. Dev Cell *21*, 559-574. S1534-
836 5807(11)00306-6 [pii]10.1016/j.devcel.2011.07.014.

837 Ginestier, C., Hur, M.H., Charafe-Jauffret, E., Monville, F., Dutcher, J., Brown, M., Jacquemier, J.,
838 Viens, P., Kleer, C.G., Liu, S., et al. (2007). ALDH1 is a marker of normal and malignant human
839 mammary stem cells and a predictor of poor clinical outcome. Cell Stem Cell *1*, 555-567.
840 10.1016/j.stem.2007.08.014.
841

842 Grieshammer, U., Cebrian, C., Ilagan, R., Meyers, E., Herzlinger, D., and Martin, G.R. (2005). FGF8 is
843 required for cell survival at distinct stages of nephrogenesis and for regulation of gene expression in
844 nascent nephrons. Development *132*, 3847-3857. dev.01944 [pii]10.1242/dev.01944.

845 Hastie, N.D. (2017). Wilms' tumour 1 (WT1) in development, homeostasis and disease. Development
846 *144*, 2862-2872. 10.1242/dev.153163.

847 Hohenstein, P., and Hastie, N.D. (2006). The many facets of the Wilms' tumour gene, WT1. Hum Mol
848 Genet *15 Spec No 2*, R196-201. 15/suppl_2/R196 [pii]10.1093/hmg/ddl196.

849 Hohenstein, P., Pritchard-Jones, K., and Charlton, J. (2015). The yin and yang of kidney development
850 and Wilms' tumors. Genes Dev *29*, 467-482. 10.1101/gad.256396.114.
851
852 Kobayashi, A., Mugford, J.W., Krautzberger, A.M., Naiman, N., Liao, J., and McMahon, A.P. (2014).
853 Identification of a Multipotent Self-Renewing Stromal Progenitor Population during Mammalian
854 Kidney Organogenesis. Stem Cell Reports *3*, 650-662. 10.1016/j.stemcr.2014.08.008.
855

856 Kobayashi, A., Valerius, M.T., Mugford, J.W., Carroll, T.J., Self, M., Oliver, G., and McMahon, A.P.
857 (2008). Six2 defines and regulates a multipotent self-renewing nephron progenitor population
858 throughout mammalian kidney development. Cell Stem Cell *3*, 169-181. S1934-5909(08)00347-0
859 [pii]10.1016/j.stem.2008.05.020.

860 Kreidberg, J.A., Sariola, H., Loring, J.M., Maeda, M., Pelletier, J., Housman, D., and Jaenisch, R.
861 (1993). WT-1 is required for early kidney development. Cell *74*, 679-691.
862 https://doi.org/10.1016/0092-8674(93)90515-R.
863
864 Li, M., Chen, H., and Wu, T. (2019). LIN28: A cancer stem cell promoter for immunotherapy in head
865 and neck squamous cell carcinoma. Oral Oncol *98*, 92-95. 10.1016/j.oraloncology.2019.09.024.
866
867 Li, Y., Gong, H., Ding, J., Zhao, F., Du, J., Wan, J., Zhang, J., Liu, S., Li, J., Wang, L., and Zhou, B. (2020).
868 Inhibition of GSK3 Represses the Expression of Retinoic Acid Synthetic Enzyme ALDH1A2 via Wnt/β-
869 Catenin Signaling in WiT49 Cells. Frontiers in Cell and Developmental Biology *8*.
870 10.3389/fcell.2020.00094.
871
872 Li, Y., Wang, L., Ai, W., He, N., Zhang, L., Du, J., Wang, Y., Mao, X., Ren, J., Xu, D., et al. (2017).
873 Regulation of retinoic acid synthetic enzymes by WT1 and HDAC inhibitors in 293 cells. Int J Mol Med
874 *40*, 661-672. 10.3892/ijmm.2017.3051.
875
876 Lindstrom, N.O., Guo, J., Kim, A.D., Tran, T., Guo, Q., De Sena Brandine, G., Ransick, A., Parvez, R.K.,
877 Thornton, M.E., Baskin, L., et al. (2018a). Conserved and Divergent Features of Mesenchymal
878 Progenitor Cell Types within the Cortical Nephrogenic Niche of the Human and Mouse Kidney. J Am
879 Soc Nephrol *29*, 806-824. 10.1681/ASN.2017080890.
880
881 Lindstrom, N.O., McMahon, J.A., Guo, J., Tran, T., Guo, Q., Rutledge, E., Parvez, R.K., Saribekyan, G.,
882 Schuler, R.E., Liao, C., et al. (2018b). Conserved and Divergent Features of Human and Mouse Kidney
883 Organogenesis. J Am Soc Nephrol *29*, 785-805. 10.1681/ASN.2017080887.
884
885 Lovvorn, H.N., Westrup, J., Opperman, S., Boyle, S., Shi, G., Anderson, J., Perlman, E.J., Perantoni,
886 A.O., Wills, M., and de Caestecker, M. (2007). CITED1 expression in Wilms' tumor and embryonic
887 kidney. Neoplasia *9*, 589-600. 10.1593/neo.07358.
888
889 Madisen, L., Garner, A.R., Shimaoka, D., Chuong, A.S., Klapoetke, N.C., Li, L., van der Bourg, A., Niino,
890 Y., Egolf, L., Monetti, C., et al. (2015). Transgenic mice for intersectional targeting of neural sensors
891 and effectors with high specificity and performance. Neuron *85*, 942-958.
892 10.1016/j.neuron.2015.02.022.
893
894 Madisen, L., Zwingman, T.A., Sunkin, S.M., Oh, S.W., Zariwala, H.A., Gu, H., Ng, L.L., Palmiter, R.D.,
895 Hawrylycz, M.J., Jones, A.R., et al. (2010). A robust and high-throughput Cre reporting and

896 characterization system for the whole mouse brain. Nature neuroscience *13*, 133-140.
897 10.1038/nn.2467.
898
899 Majumdar, A., Vainio, S., Kispert, A., McMahon, J., and McMahon, A.P. (2003). Wnt11 and Ret/Gdnf
900 pathways cooperate in regulating ureteric branching during metanephric kidney development.
901 Development *130*, 3175-3185.
902
903 Markovic-Lipkovski, J., Muller, C.A., Klein, G., Flad, T., Klatt, T., Blaschke, S., Wessels, J.T., and Muller,
904 G.A. (2007). Neural cell adhesion molecule expression on renal interstitial cells. Nephrol Dial
905 Transplant *22*, 1558-1566. 10.1093/ndt/gfm006.
906
907 Martinez-Estrada, O.M., Lettice, L.A., Essafi, A., Guadix, J.A., Slight, J., Velecela, V., Hall, E.,
908 Reichmann, J., Devenney, P.S., Hohenstein, P., et al. (2010). Wt1 is required for cardiovascular
909 progenitor cell formation through transcriptional control of Snail and E-cadherin. Nat Genet *42*, 89-
910 93. ng.494 [pii]10.1038/ng.494.
911
912 McMahon, A.P. (2016). Development of the Mammalian Kidney. Curr Top Dev Biol *117*, 31-64.
913 10.1016/bs.ctdb.2015.10.010.
914
915 Miyagawa, K., Kent, J., Moore, A., Charlieu, J.P., Little, M.H., Williamson, K.A., Kelsey, A., Brown,
916 K.W., Hassam, S., Briner, J., et al. (1998). Loss of WT1 function leads to ectopic myogenesis in Wilms'
917 tumour. Nat Genet *18*, 15-17. 10.1038/ng0198-15.
918
919 Mugford, J.W., Sipila, P., Kobayashi, A., Behringer, R.R., and McMahon, A.P. (2008). Hoxd11 specifies
920 a program of metanephric kidney development within the intermediate mesoderm of the mouse
921 embryo. Dev Biol *319*, 396-405. 10.1016/j.ydbio.2008.03.044.
922
923 Mugford, J.W., Yu, J., Kobayashi, A., and McMahon, A.P. (2009). High-resolution gene expression
924 analysis of the developing mouse kidney defines novel cellular compartments within the nephron
925 progenitor population. Dev Biol *333*, 312-323. 10.1016/j.ydbio.2009.06.043.
926
927 Murphy, A.J., Pierce, J., de Caestecker, C., Taylor, C., Anderson, J.R., Perantoni, A.O., de Caestecker,
928 M.P., and Lovvorn, H.N., 3rd (2012). SIX2 and CITED1, markers of nephronic progenitor self-renewal,
929 remain active in primitive elements of Wilms' tumor. Journal of pediatric surgery *47*, 1239-1249.
930 10.1016/j.jpedsurg.2012.03.034.
931
932 Naiman, N., Fujioka, K., Fujino, M., Valerius, M.T., Potter, S.S., McMahon, A.P., and Kobayashi, A.
933 (2017). Repression of Interstitial Identity in Nephron Progenitor Cells by Pax2 Establishes the
934 Nephron-Interstitium Boundary during Kidney Development. Dev Cell *41*, 349-365 e343.
935 10.1016/j.devcel.2017.04.022.
936
937 Niculovic, K.M., Vicente, M.M., Wittek, V., Kats, E., Albers, I., Flachsig-Schulz, K., Peters-Bernard, U.,
938 Weiss, A.C., Thiesler, H., Drager, L.S., et al. (2025). Polysialic acid regulates glomerular
939 microvasculature formation by interaction with VEGF-A188 in mice. Angiogenesis *28*, 31.
940 10.1007/s10456-025-09984-6.
941
942 Niederreither, K., Subbarayan, V., Dollé, P., and Chambon, P. (1999). Embryonic retinoic acid
943 synthesis is essential for early mouse post-implantation development. Nature Genetics *21*, 444-448.
944 10.1038/7788.
945

946 O'Brien, L.L., Guo, Q., Bahrami-Samani, E., Park, J.S., Hasso, S.M., Lee, Y.J., Fang, A., Kim, A.D., Guo,
947 J., Hong, T.M., et al. (2018). Transcriptional regulatory control of mammalian nephron progenitors
948 revealed by multi-factor cistromic analysis and genetic studies. PLoS Genet *14*, e1007181.
949 10.1371/journal.pgen.1007181.
950
951 Petrosyan, A., Villani, V., Aguiari, P., Thornton, M.E., Wang, Y., Rajewski, A., Zhou, S., Cravedi, P.,
952 Grubbs, B.H., De Filippo, R.E., et al. (2023). Identification and Characterization of the Wilms Tumor
953 Cancer Stem Cell. Adv Sci (Weinh), e2206787. 10.1002/advs.202206787.
954
955 Pode-Shakked, N., Metsuyanim, S., Rom-Gross, E., Mor, Y., Fridman, E., Goldstein, I., Amariglio, N.,
956 Rechavi, G., Keshet, G., and Dekel, B. (2009). Developmental tumourigenesis: NCAM as a putative
957 marker for the malignant renal stem/progenitor cell population. J Cell Mol Med *13*, 1792-1808.
958 10.1111/j.1582-4934.2008.00607.x.
959
960 Pode-Shakked, N., Shukrun, R., Mark-Danieli, M., Tsvetkov, P., Bahar, S., Pri-Chen, S., Goldstein, R.S.,
961 Rom-Gross, E., Mor, Y., Fridman, E., et al. (2013). The isolation and characterization of renal cancer
962 initiating cells from human Wilms' tumour xenografts unveils new therapeutic targets. EMBO Mol
963 Med *5*, 18-37. 10.1002/emmm.201201516.
964
965 Royer-Pokora, B., Wruck, W., Adjaye, J., and Beier, M. (2023). Gene expression studies of WT1
966 mutant Wilms tumor cell lines in the frame work of published kidney development data reveals their
967 early kidney stem cell origin. PLoS One *18*, e0270380. 10.1371/journal.pone.0270380.
968
969 Schumacher, V., Schuhen, S., Sonner, S., Weirich, A., Leuschner, I., Harms, D., Licht, J., Roberts, S.,
970 and Royer-Pokora, B. (2003). Two molecular subgroups of Wilms' tumors with or without WT1
971 mutations. Clin Cancer Res *9*, 2005-2014.
972
973 Shukrun, R., Pode-Shakked, N., Pleniceanu, O., Omer, D., Vax, E., Peer, E., Pri-Chen, S., Jacob, J., Hu,
974 Q., Harari-Steinberg, O., et al. (2014). Wilms' tumor blastemal stem cells dedifferentiate to
975 propagate the tumor bulk. Stem Cell Reports *3*, 24-33. 10.1016/j.stemcr.2014.05.013S2213-
976 6711(14)00154-4 [pii].
977 Spreafico, F., Fernandez, C.V., Brok, J., Nakata, K., Vujanic, G., Geller, J.I., Gessler, M., Maschietto, M.,
978 Behjati, S., Polanco, A., et al. (2021). Wilms tumour. Nat Rev Dis Primers *7*, 75. 10.1038/s41572-021-
979 00308-8.
980
981 Urbach, A., Yermalovich, A., Zhang, J., Spina, C.S., Zhu, H., Perez-Atayde, A.R., Shukrun, R., Charlton,
982 J., Sebire, N., Mifsud, W., et al. (2014). Lin28 sustains early renal progenitors and induces Wilms
983 tumor. Genes Dev *28*, 971-982. 10.1101/gad.237149.113.
984
985 Viswanathan, S.R., and Daley, G.Q. (2010). Lin28: A microRNA regulator with a macro role. Cell *140*,
986 445-449. 10.1016/j.cell.2010.02.007.
987
988 Wegert, J., Zauter, L., Appenzeller, S., Otto, C., Bausenwein, S., Vokuhl, C., Ernestus, K., Furtwangler,
989 R., Graf, N., and Gessler, M. (2020). High-risk blastemal Wilms tumor can be modeled by 3D spheroid
990 cultures in vitro. Oncogene *39*, 849-861. 10.1038/s41388-019-1027-8.
991
992 Weiss, A.C., Rivera-Reyes, R., Englert, C., and Kispert, A. (2020). Expansion of the renal capsular
993 stroma, ureteric bud branching defects and cryptorchidism in mice with Wilms tumor 1 gene
994 deletion in the stromal compartment of the developing kidney. J Pathol *252*, 290-303.
995 10.1002/path.5518.

Yermalovich, A.V., Osborne, J.K., Sousa, P., Han, A., Kinney, M.A., Chen, M.J., Robinton, D.A., Montie, H., Pearson, D.S., Wilson, S.B., et al. (2019). Lin28 and let-7 regulate the timing of cessation of murine nephrogenesis. Nat Commun *10*, 168. 10.1038/s41467-018-08127-4.

Zheng, H., Liu, J., Pan, X., and Cui, X. (2023). Biomarkers for patients with Wilms tumor: a review. Front Oncol *13*, 1137346. 10.3389/fonc.2023.1137346.

Zhou, B., Ma, Q., Rajagopal, S., Wu, S.M., Domian, I., Rivera-Feliciano, J., Jiang, D., von Gise, A., Ikeda, S., Chien, K.R., and Pu, W.T. (2008). Epicardial progenitors contribute to the cardiomyocyte lineage in the developing heart. Nature *454*, 109-113. 10.1038/nature07060nature07060 [pii].

Zhou, J., Ng, S.B., and Chng, W.J. (2013). LIN28/LIN28B: an emerging oncogenic driver in cancer stem cells. The international journal of biochemistry & cell biology *45*, 973-978. 10.1016/j.biocel.2013.02.006.

Zhou, L., Sheng, D., Wang, D., Ma, W., Deng, Q., Deng, L., and Liu, S. (2019). Identification of cancer-type specific expression patterns for active aldehyde dehydrogenase (ALDH) isoforms in ALDEFLUOR assay. Cell Biol Toxicol *35*, 161-177. 10.1007/s10565-018-9444-y.

Figure1

A.

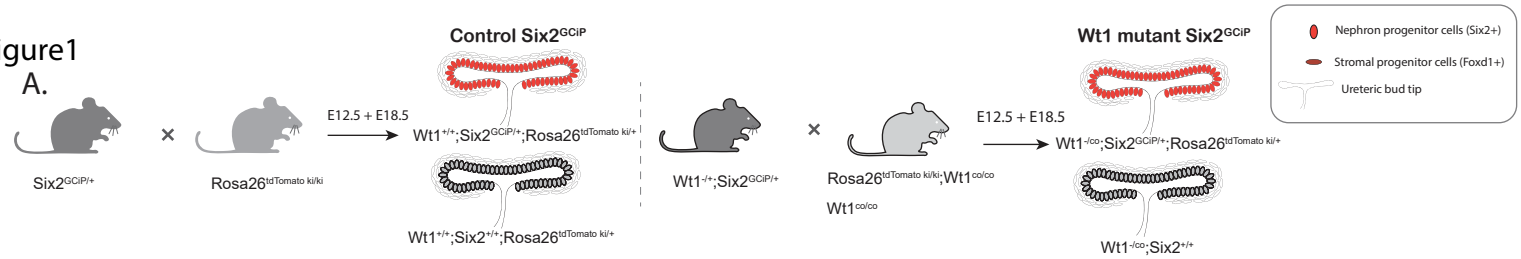

B.

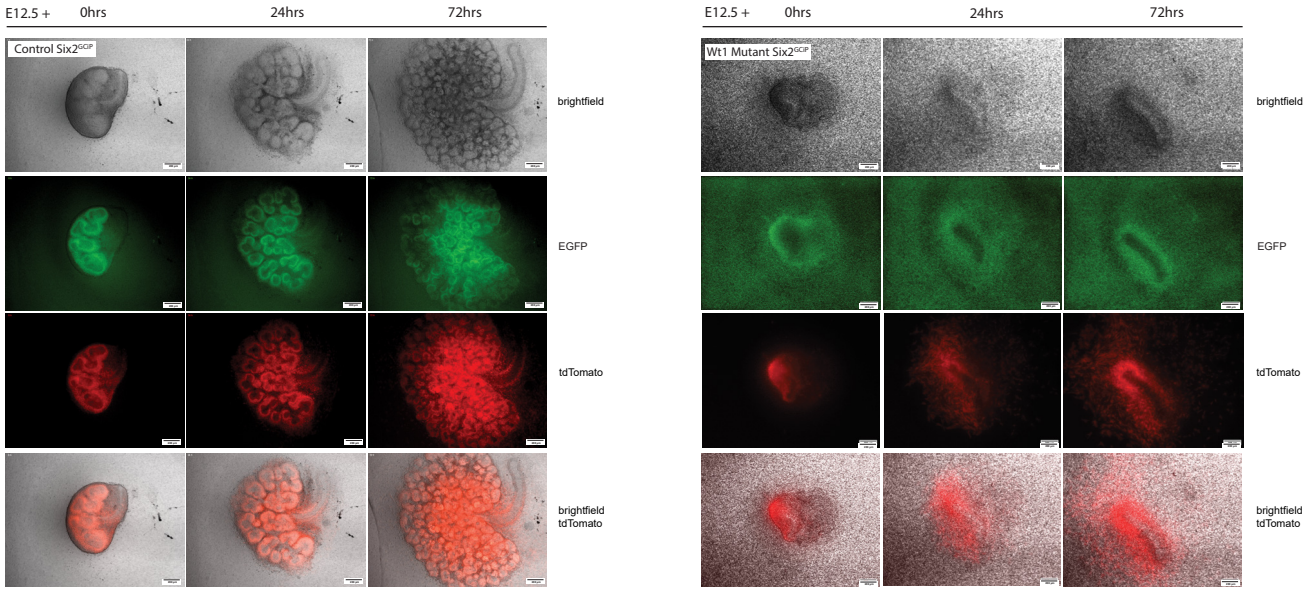

C.

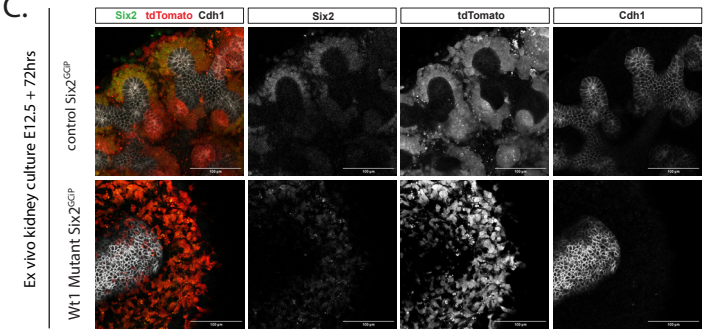

D.

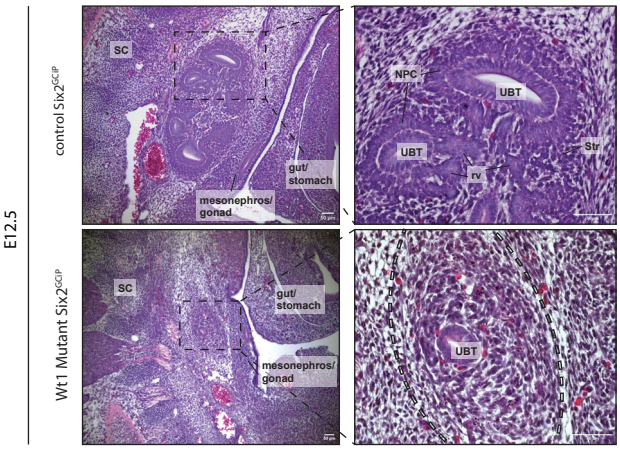

E.

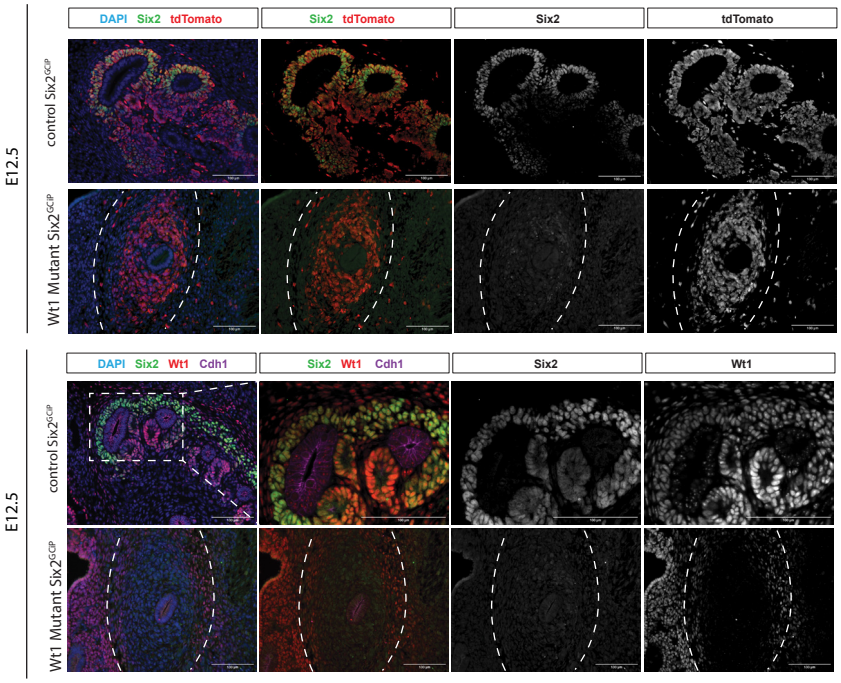

F.

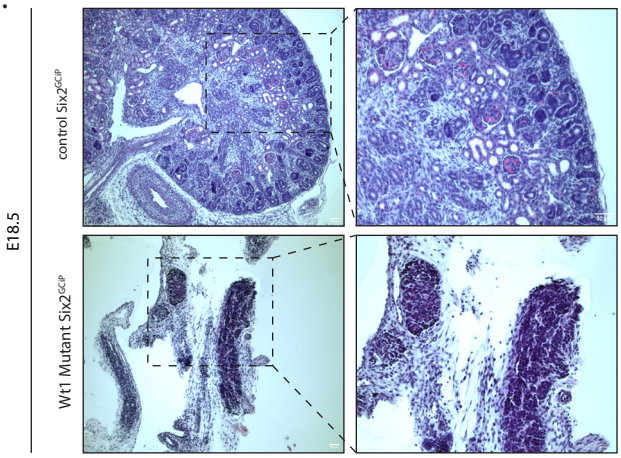

G.

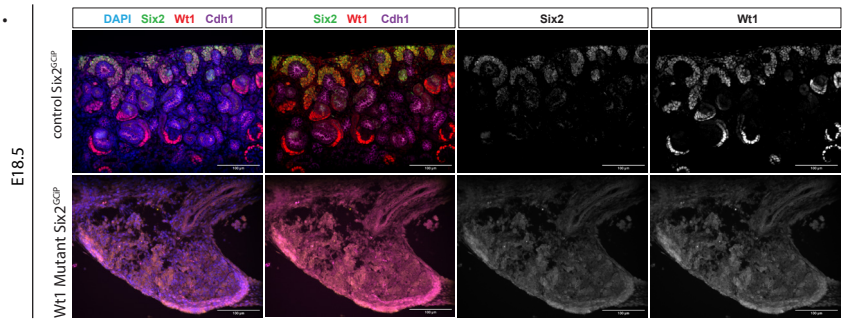

Figure 2

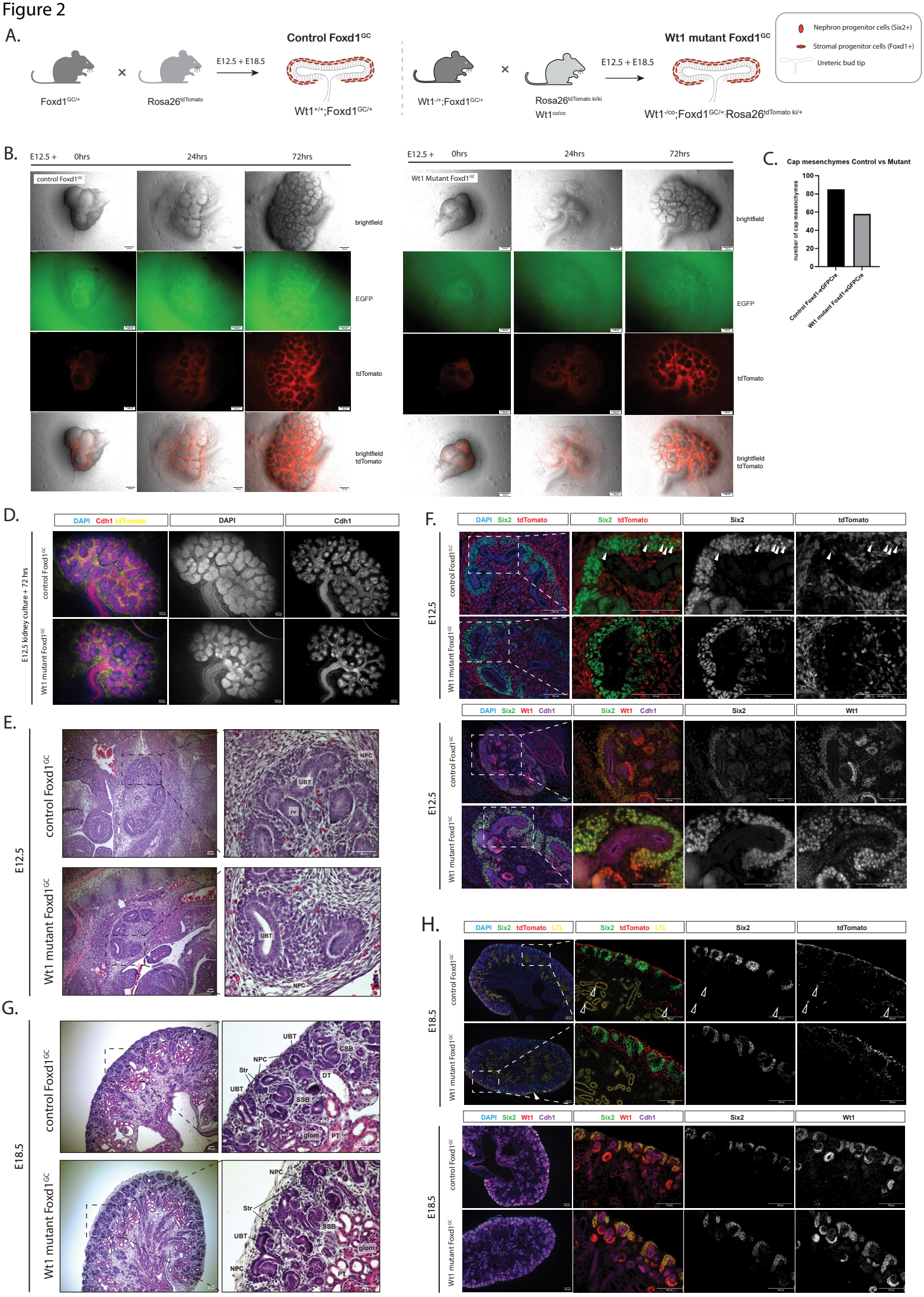
A.
Control Foxd1GC
Foxd1GC/+
Rosa26tdTomato
E12.5 + E18.5
Wt1+/+;Foxd1GC/+
Wt1 mutant Foxd1GC
Wt1-/+;Foxd1GC/+
Rosa26tdTomato ki/ki
Wt1co/co
Wt1-/co;Foxd1GC/+;Rosa26tdTomato ki/+
Nephron progenitor cells (Six2+)
Stromal progenitor cells (Foxd1+)
Ureteric bud tip
B.
E12.5 +
0hrs
24hrs
72hrs
control Foxd1GC
Wt1 Mutant Foxd1GC
brightfield
EGFP
tdTomato
brightfield tdTomato
C.
Cap mesenchymes Control vs Mutant
number of cap mesenchymes
100
80
60
40
20
0
Control Foxd1-eGFPCre
Wt1 mutant Foxd1-eGFPCre
D.
E12.5 kidney culture + 72 hrs
DAPI Cdh1 tdTomato
DAPI
Cdh1
control Foxd1GC
Wt1 mutant Foxd1GC
E.
E12.5
control Foxd1GC
Wt1 mutant Foxd1GC
NPC
UBT
rv
G.
E18.5
control Foxd1GC
Wt1 mutant Foxd1GC
UBT
NPC
Str
CSB
DT
SSB
glom
PT
F.
DAPI Six2 tdTomato
Six2 tdTomato
Six2
tdTomato
DAPI Six2 Wt1 Cdh1
Six2 Wt1 Cdh1
Wt1
H.
DAPI Six2 tdTomato LTL
Six2 tdTomato LTL

Figure 3

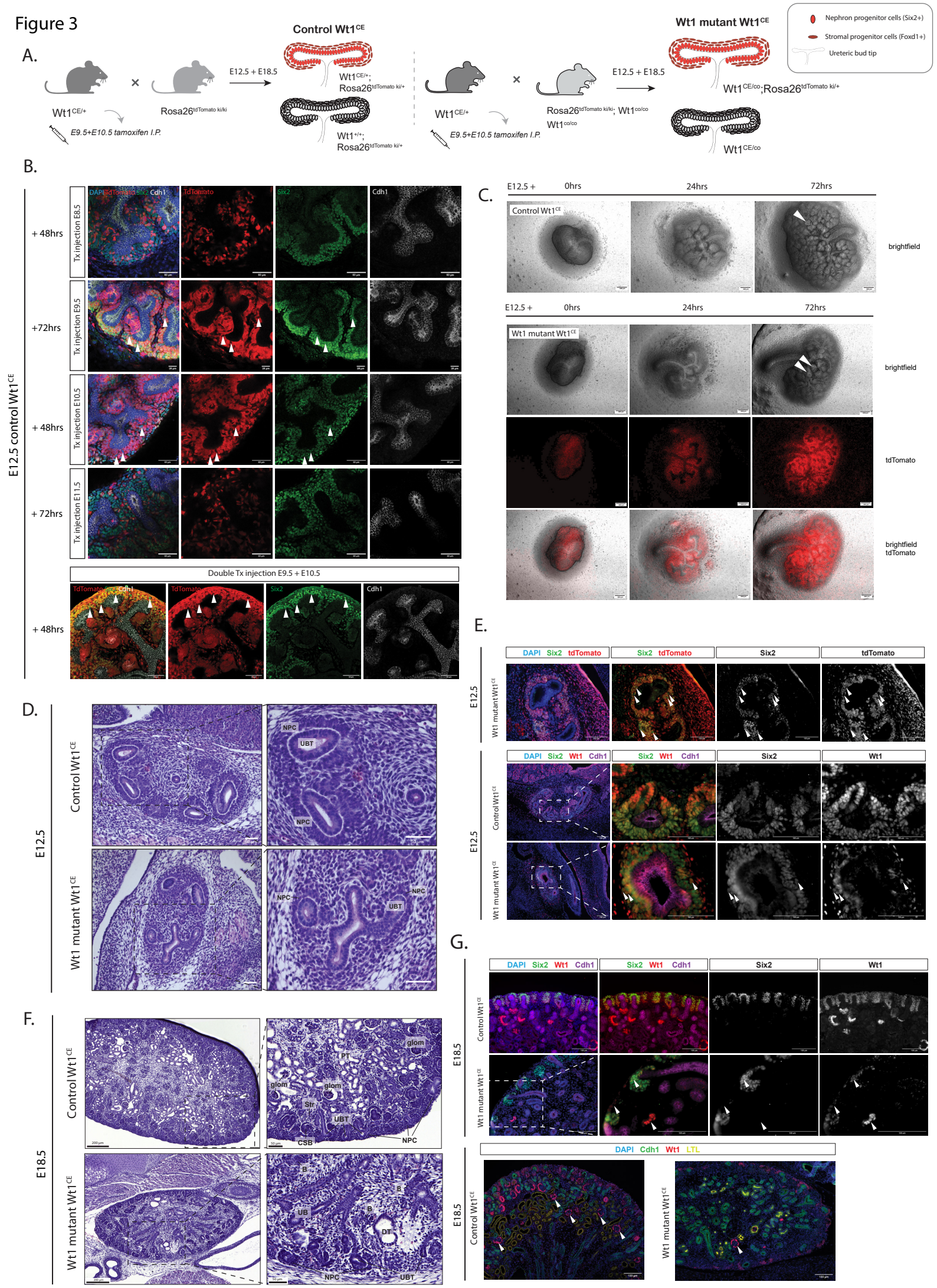
A.
Control Wt1CE
Wt1 mutant Wt1CE
Nephron progenitor cells (Six2+)
Stromal progenitor cells (Foxd1+)
Ureteric bud tip
Wt1CE/+
Rosa26tdTomato ki/ki
E9.5+E10.5 tamoxifen I.P.
E12.5 + E18.5
Wt1CE/+; Rosa26tdTomato ki/+
Wt1+/+; Rosa26tdTomato ki/+
Rosa26tdTomato ki/ki; Wt1co/co
Wt1co/co
Wt1CE/co;Rosa26tdTomato ki/+
Wt1CE/co
B.
E12.5 control Wt1CE
+ 48hrs
Tx injection E8.5
+72hrs
Tx injection E9.5
+ 48hrs
Tx injection E10.5
+ 72hrs
Tx injection E11.5
Double Tx injection E9.5 + E10.5
+ 48hrs
DAPI TdTomato Six2 Cdh1
TdTomato
Six2
Cdh1
C.
E12.5 +
0hrs
24hrs
72hrs
Control Wt1CE
Wt1 mutant Wt1CE
brightfield
tdTomato
brightfield tdTomato
D.
E12.5
Control Wt1CE
Wt1 mutant Wt1CE
NPC
UBT
E.
E12.5
DAPI Six2 tdTomato
Six2 tdTomato
Six2
tdTomato
DAPI Six2 Wt1 Cdh1
Six2 Wt1 Cdh1
Six2
Wt1
F.
E18.5
Control Wt1CE
Wt1 mutant Wt1CE
glom
PT
Str
UBT
CSB
NPC
B
UB
DT
G.
E18.5
DAPI Six2 Wt1 Cdh1
Six2 Wt1 Cdh1
Six2
Wt1
DAPI Cdh1 Wt1 LTL

Figure 4

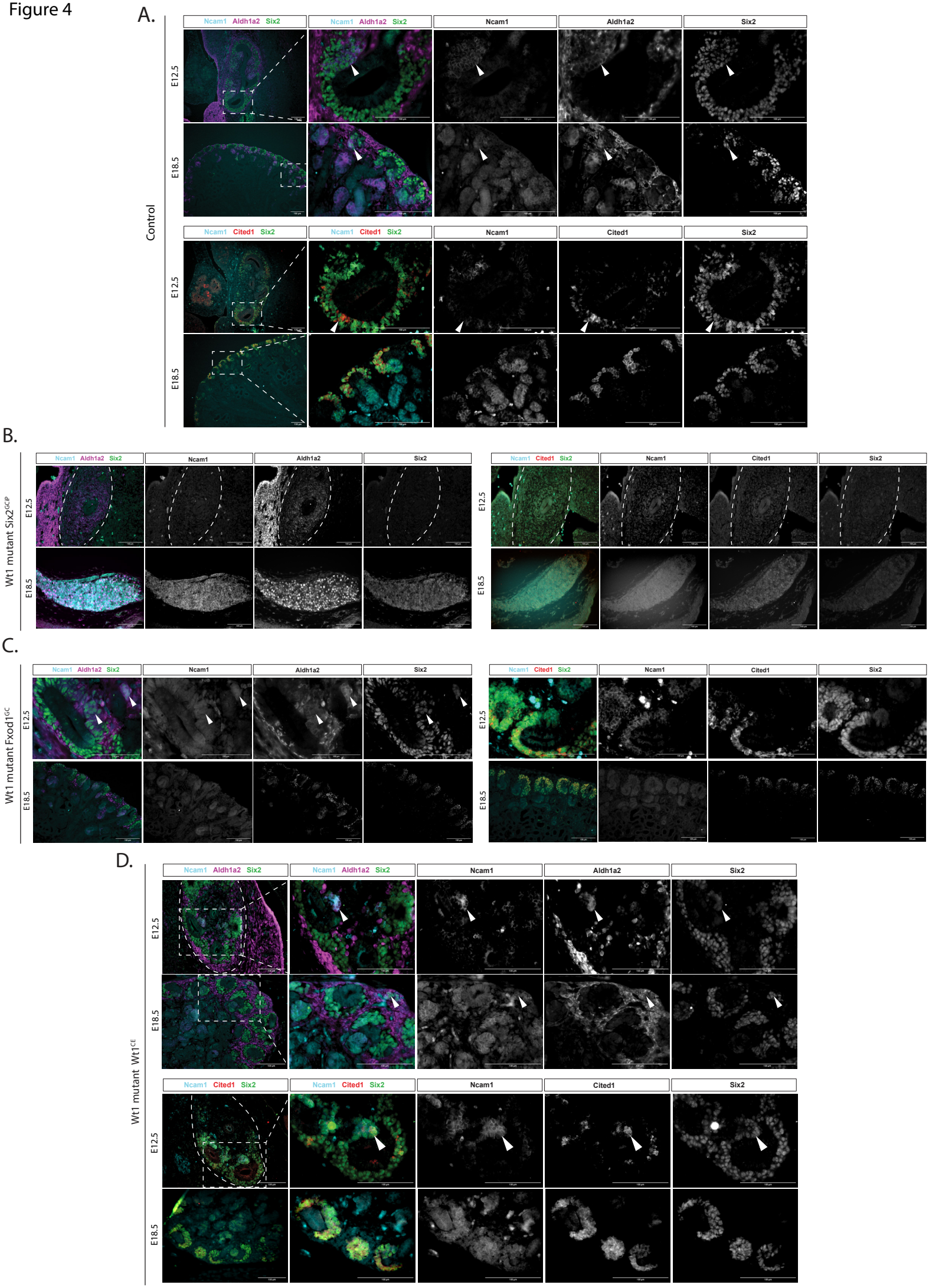
A.
Control
E12.5
E18.5
Ncam1 Aldh1a2 Six2
Ncam1 Aldh1a2 Six2
Ncam1
Aldh1a2
Six2
Ncam1 Cited1 Six2
Ncam1 Cited1 Six2
Ncam1
Cited1
Six2
B.
Wt1 mutant Six2GCIP
E12.5
E18.5
Ncam1 Aldh1a2 Six2
Ncam1
Aldh1a2
Six2
Ncam1 Cited1 Six2
Ncam1
Cited1
Six2
C.
Wt1 mutant Fxod1GC
E12.5
E18.5
Ncam1 Aldh1a2 Six2
Ncam1
Aldh1a2
Six2
Ncam1 Cited1 Six2
Ncam1
Cited1
Six2
D.
Wt1 mutant Wt1CE
E12.5
E18.5
Ncam1 Aldh1a2 Six2
Ncam1 Aldh1a2 Six2
Ncam1
Aldh1a2
Six2
Ncam1 Cited1 Six2
Ncam1 Cited1 Six2
Ncam1
Cited1
Six2

Figure 5

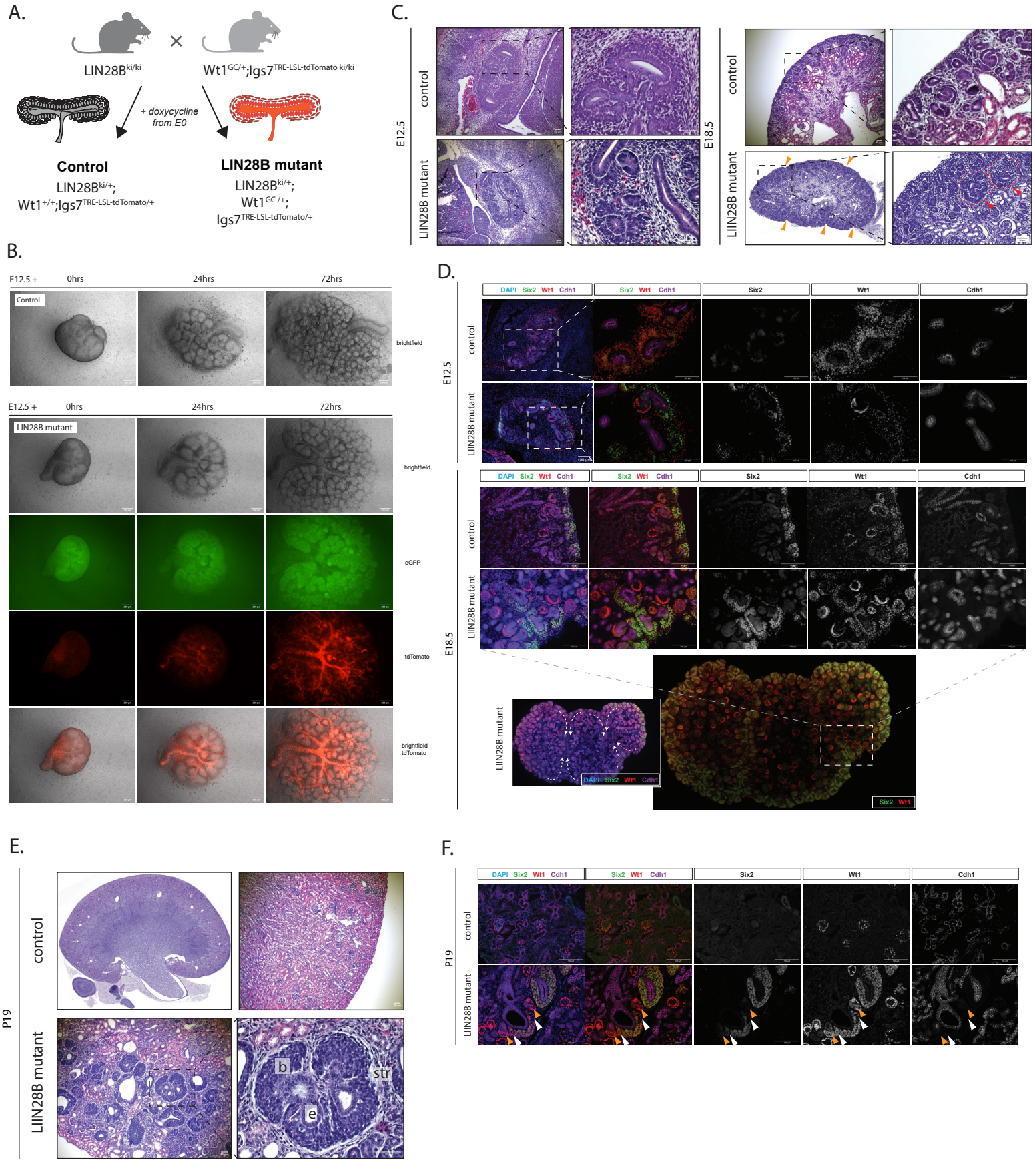
A.
LIN28B ki/ki
Wt1 GC/+;Igs7 TRE-LSL-tdTomato ki/ki
+ doxycycline from E0
Control
LIN28B ki/+; Wt1 +/+;Igs7 TRE-LSL-tdTomato/+
LIN28B mutant
LIN28B ki/+; Wt1 GC/+; Igs7 TRE-LSL-tdTomato/+
B.
E12.5 +
0hrs
24hrs
72hrs
Control
LIN28B mutant
brightfield
eGFP
tdTomato
brightfield tdTomato
C.
E12.5
E18.5
control
LIIN28B mutant
D.
DAPI Six2 Wt1 Cdh1
Six2 Wt1 Cdh1
Six2
Wt1
Cdh1
E.
P19
b
str
e
F.

Figure 6

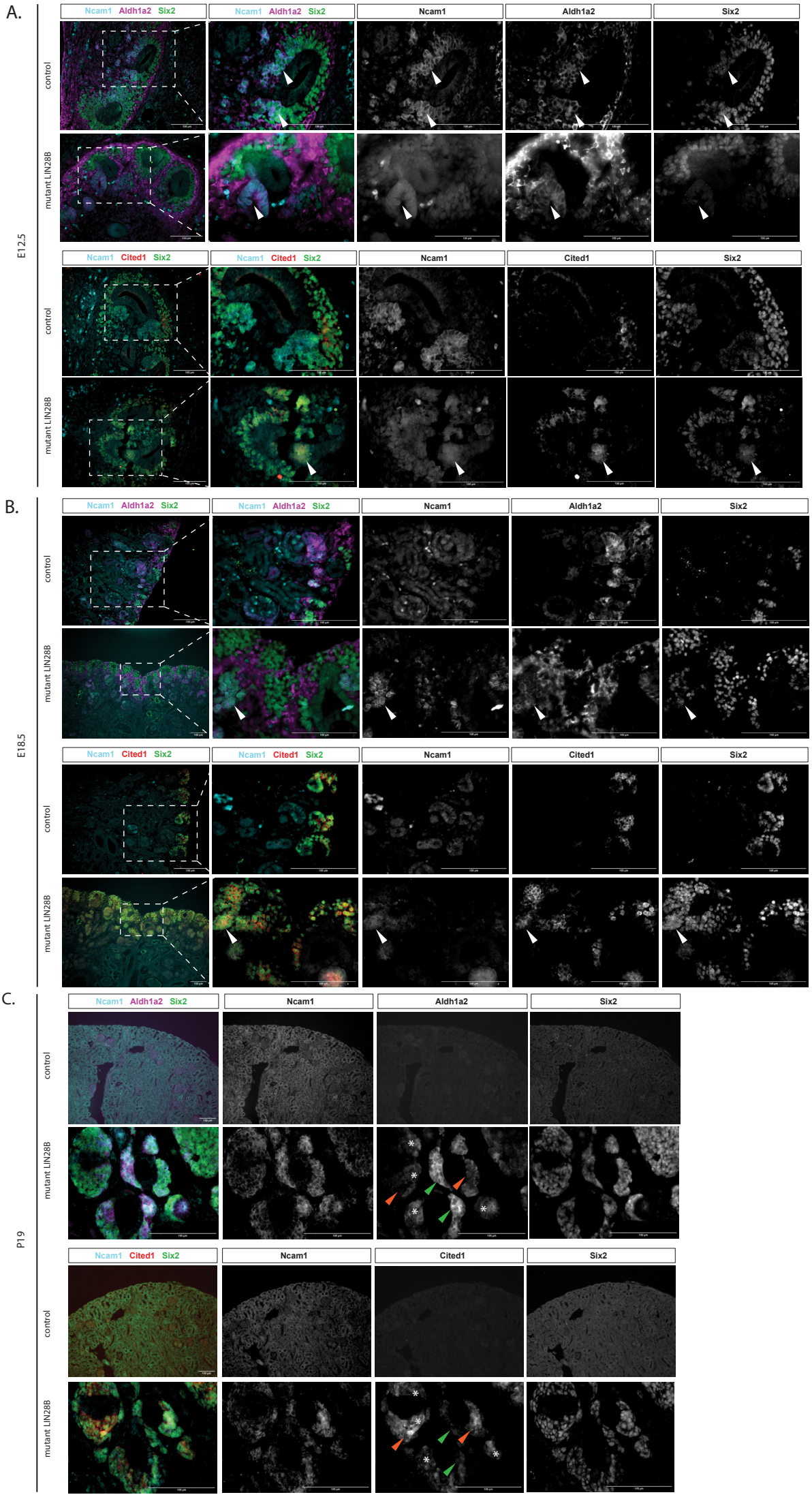
A.
E12.5
control
mutant LIN28B
Ncam1 Aldh1a2 Six2
Ncam1 Aldh1a2 Six2
Ncam1
Aldh1a2
Six2
Ncam1 Cited1 Six2
Ncam1 Cited1 Six2
Ncam1
Cited1
Six2
B.
E18.5
control
mutant LIN28B
Ncam1 Aldh1a2 Six2
Ncam1 Aldh1a2 Six2
Ncam1
Aldh1a2
Six2
Ncam1 Cited1 Six2
Ncam1 Cited1 Six2
Ncam1
Cited1
Six2
C.
P19
control
mutant LIN28B
Ncam1 Aldh1a2 Six2
Ncam1
Aldh1a2
Six2
Ncam1 Cited1 Six2
Ncam1
Cited1
Six2

Figure 7

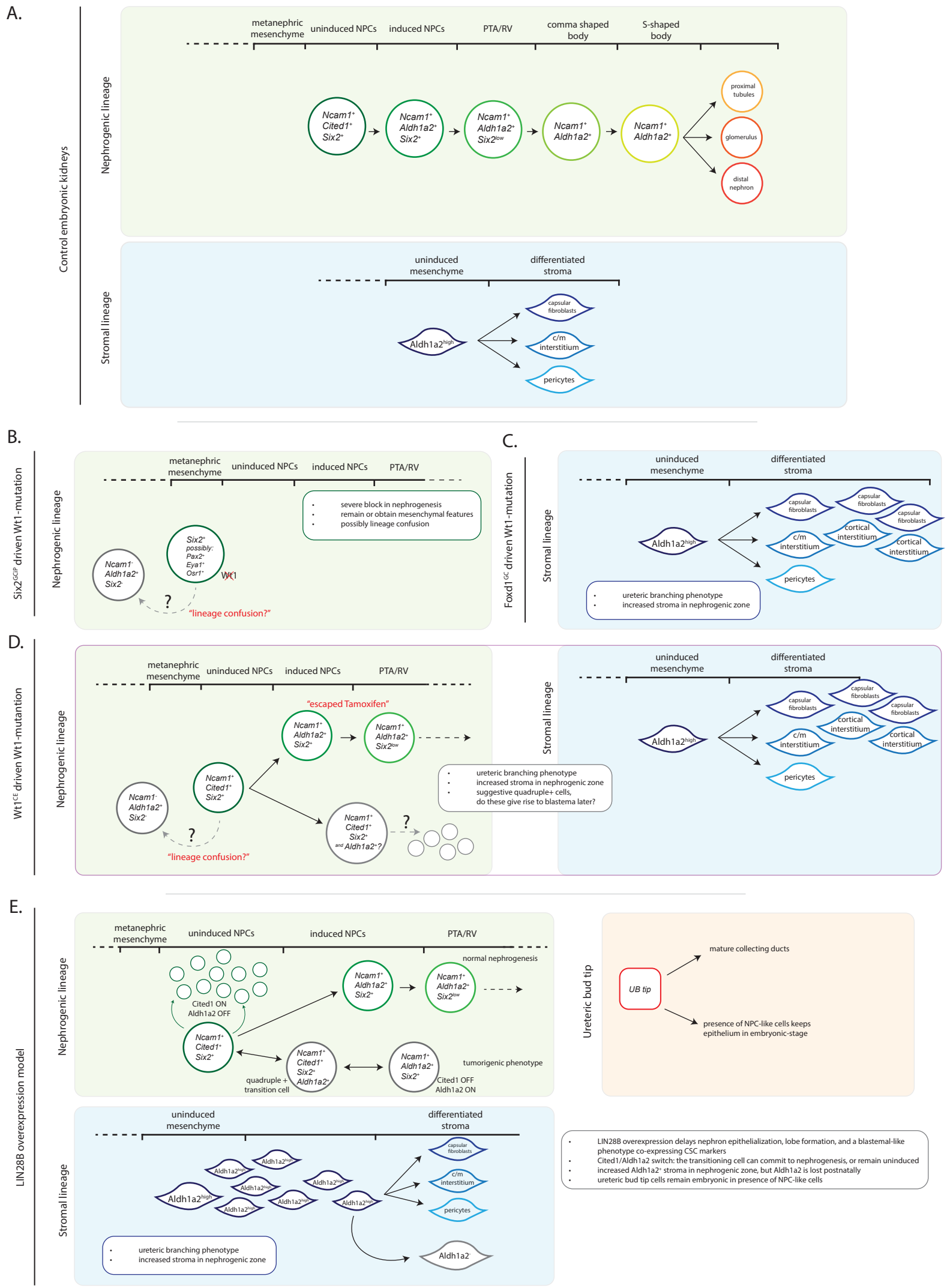
A.
Control embryonic kidneys
Nephrogenic lineage
metanephric mesenchyme
uninduced NPCs
induced NPCs
PTA/RV
comma shaped body
S-shaped body
Ncam1+ Cited1+ Six2+
Ncam1+ Aldh1a2+ Six2+
Ncam1+ Aldh1a2+ Six2low
Ncam1+ Aldh1a2+
Ncam1+ Aldh1a2+
proximal tubules
glomerulus
distal nephron
Stromal lineage
uninduced mesenchyme
differentiated stroma
Aldh1a2high
capsular fibroblasts
c/m interstitium
pericytes
B.
Six2GCIP driven Wt1-mutation
Nephrogenic lineage
metanephric mesenchyme
uninduced NPCs
induced NPCs
PTA/RV
severe block in nephrogenesis
remain or obtain mesenchymal features
possibly lineage confusion
Ncam1- Aldh1a2+ Six2-
Six2+ possibly: Pax2+ Eya1+ Osr1+
Wt1
"lineage confusion?"
C.
Foxd1GC driven Wt1-mutation
Stromal lineage
uninduced mesenchyme
differentiated stroma
Aldh1a2high
capsular fibroblasts
c/m interstitium
cortical interstitium
pericytes
ureteric branching phenotype
increased stroma in nephrogenic zone
D.
Wt1CE driven Wt1-mutantion
Nephrogenic lineage
metanephric mesenchyme
uninduced NPCs
induced NPCs
PTA/RV
"escaped Tamoxifen"
Ncam1+ Aldh1a2+ Six2+
Ncam1+ Aldh1a2+ Six2low
Ncam1+ Cited1+ Six2+
Ncam1- Aldh1a2+ Six2-
Ncam1+ Cited1+ Six2+ and Aldh1a2+?
"lineage confusion?"
ureteric branching phenotype
increased stroma in nephrogenic zone
suggestive quadruple+ cells, do these give rise to blastema later?
Stromal lineage
uninduced mesenchyme
differentiated stroma
Aldh1a2high
capsular fibroblasts
c/m interstitium
cortical interstitium
pericytes
E.
LIN28B overexpression model
Nephrogenic lineage
metanephric mesenchyme
uninduced NPCs
induced NPCs
PTA/RV
normal nephrogenesis
Cited1 ON Aldh1a2 OFF
Ncam1+ Cited1+ Six2+
Ncam1+ Aldh1a2+ Six2+
Ncam1+ Aldh1a2+ Six2low
Ncam1+ Cited1+ Six2+ Aldh1a2+
Ncam1+ Aldh1a2+ Six2+
tumorigenic phenotype
quadruple + transition cell
Cited1 OFF Aldh1a2 ON
Ureteric bud tip
UB tip
mature collecting ducts
presence of NPC-like cells keeps epithelium in embryonic-stage
Stromal lineage
uninduced mesenchyme
differentiated stroma
Aldh1a2high
capsular fibroblasts
c/m interstitium
pericytes
Aldh1a2-
ureteric branching phenotype
increased stroma in nephrogenic zone
LIN28B overexpression delays nephron epithelialization, lobe formation, and a blastemal-like phenotype co-expressing CSC markers
Cited1/Aldh1a2 switch: the transitioning cell can commit to nephrogenesis, or remain uninduced
increased Aldh1a2+ stroma in nephrogenic zone, but Aldh1a2 is lost postnatally
ureteric bud tip cells remain embryonic in presence of NPC-like cells

Supplementary Fig. 1

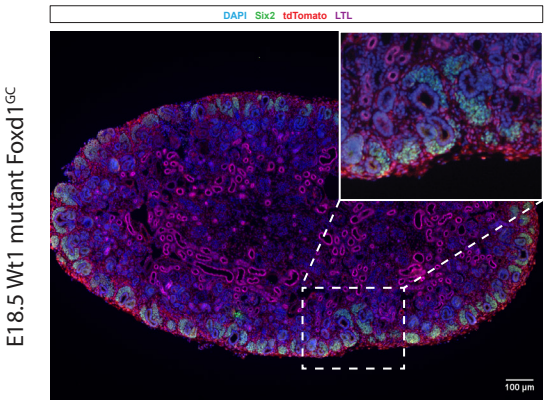

Supplementary Fig. 2

A.

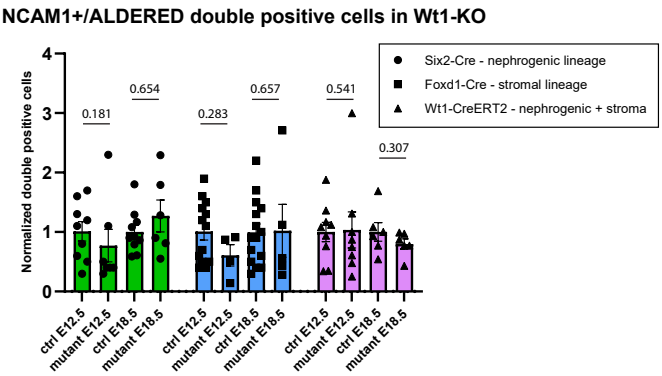

B.

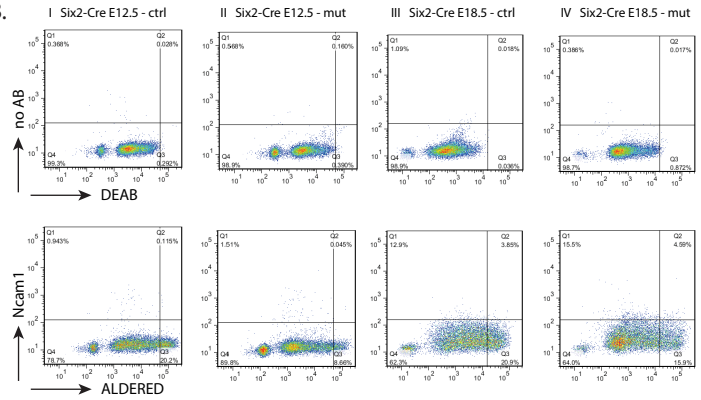

C.

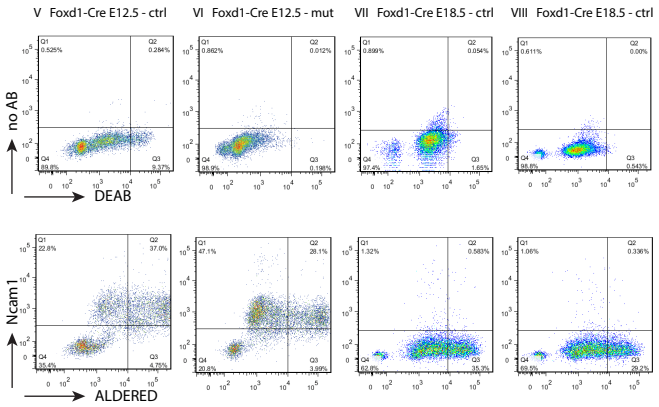

D.

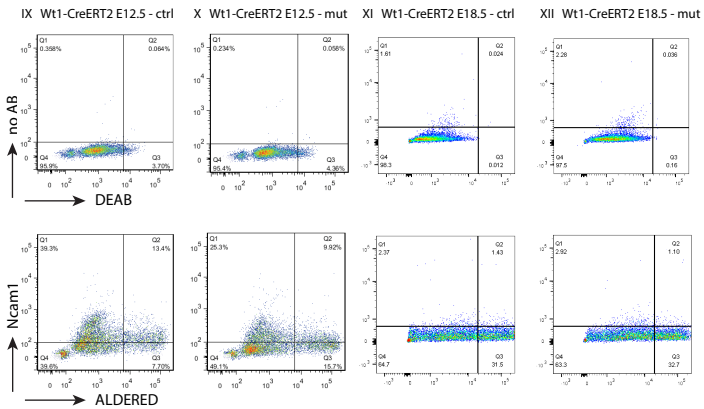

Supplementary Fig. 3

A.

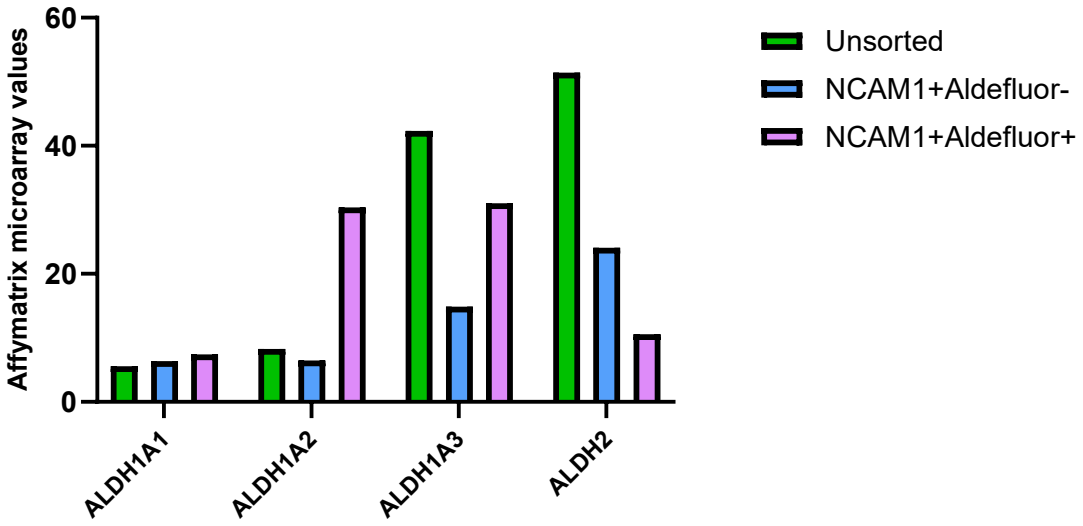

B.

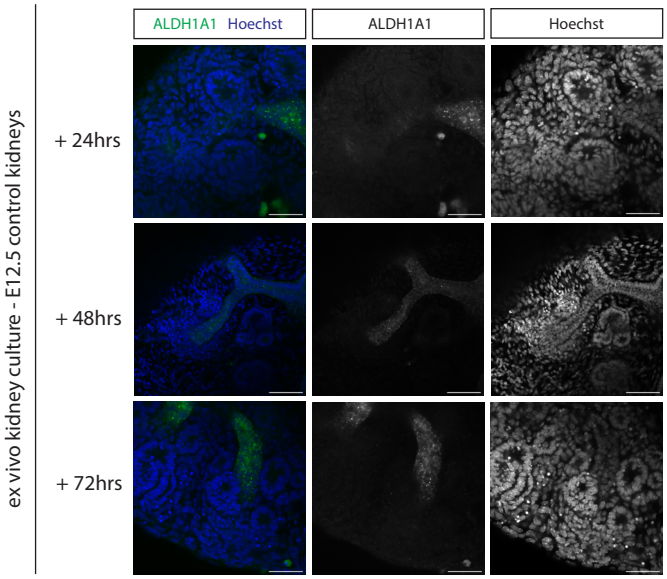

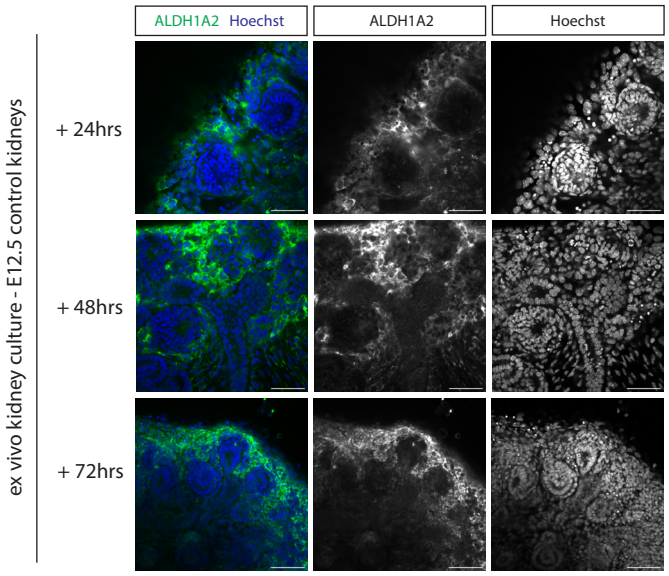

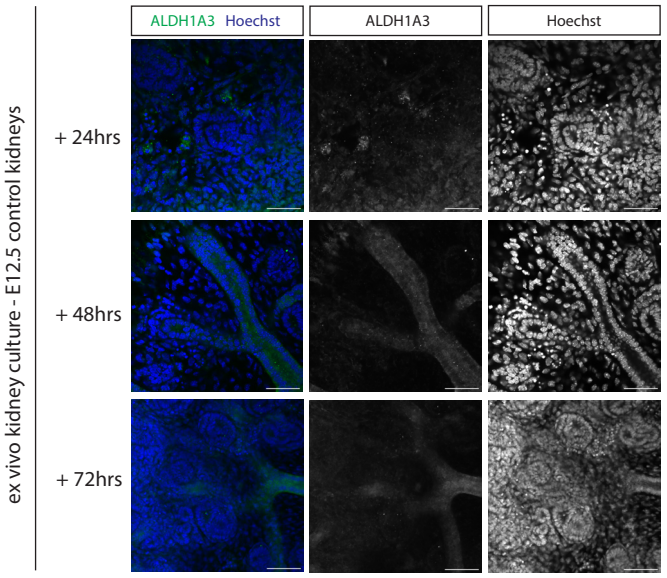

C.

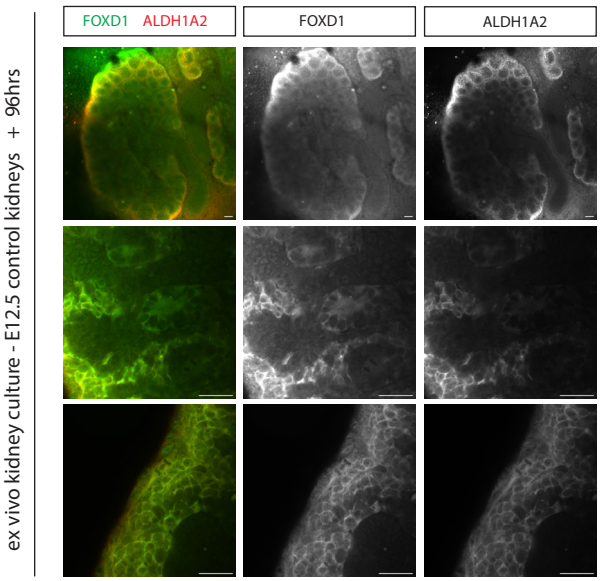

Supplementary Fig. 4

A.

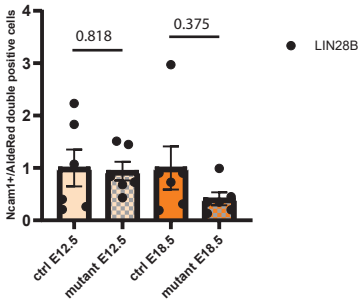

B.

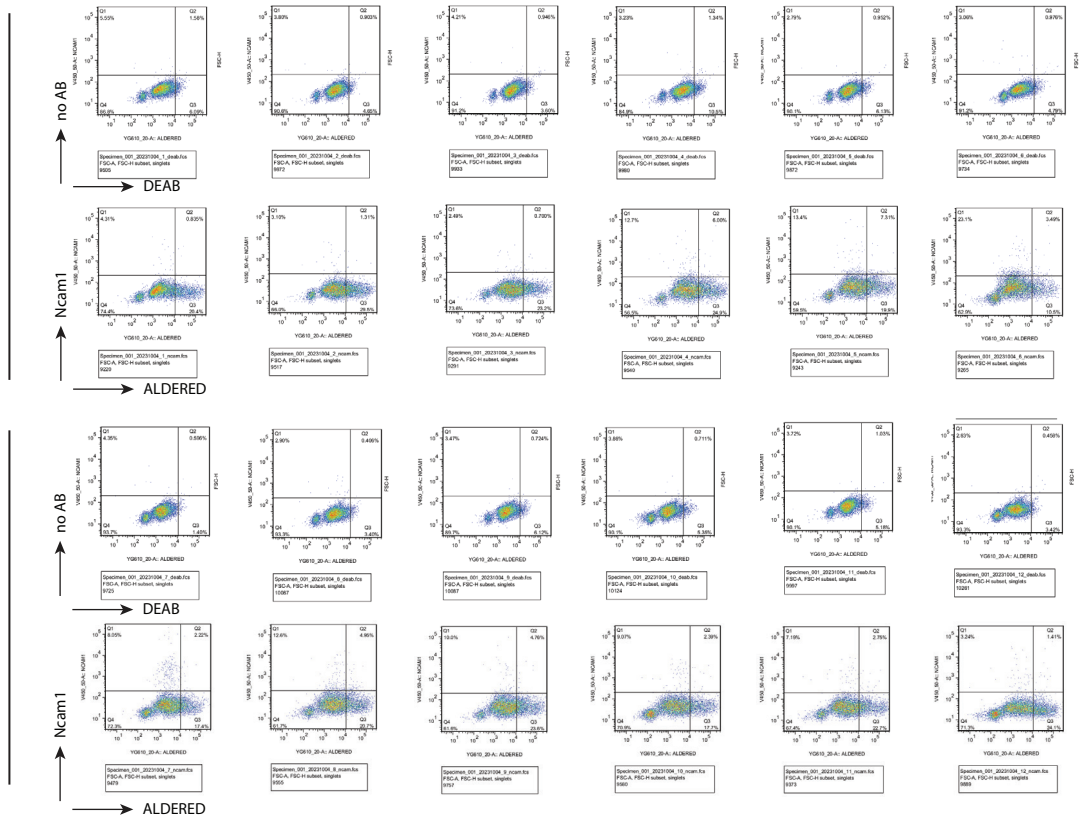

C.

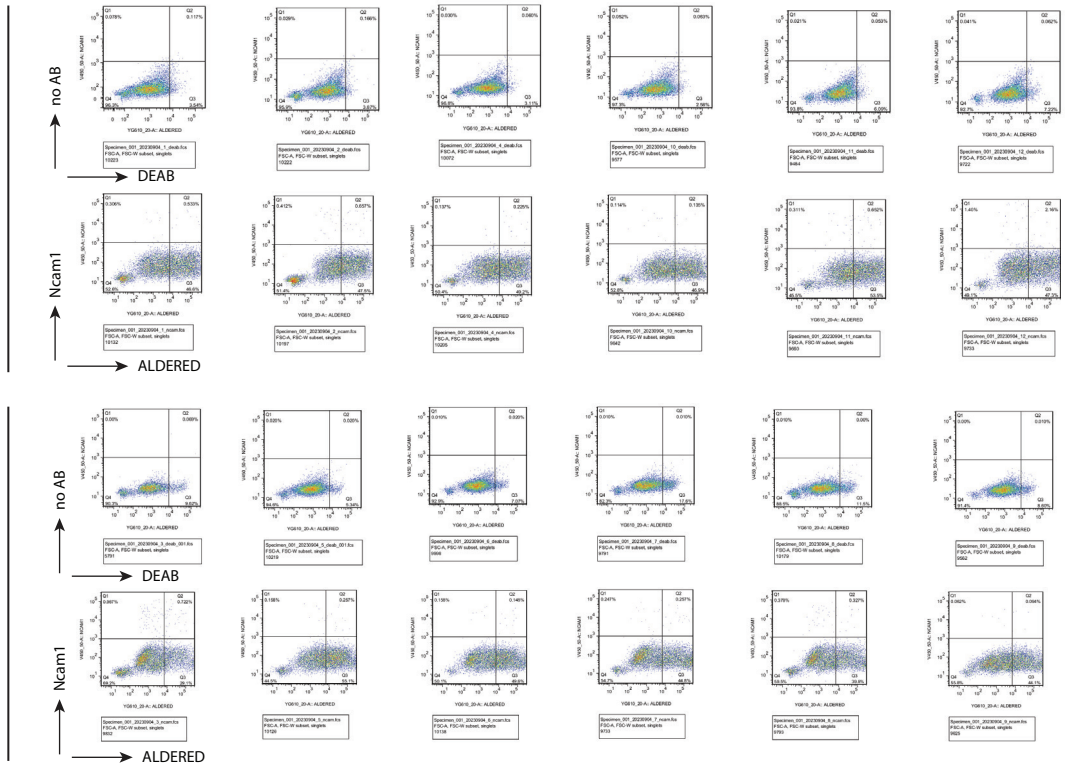
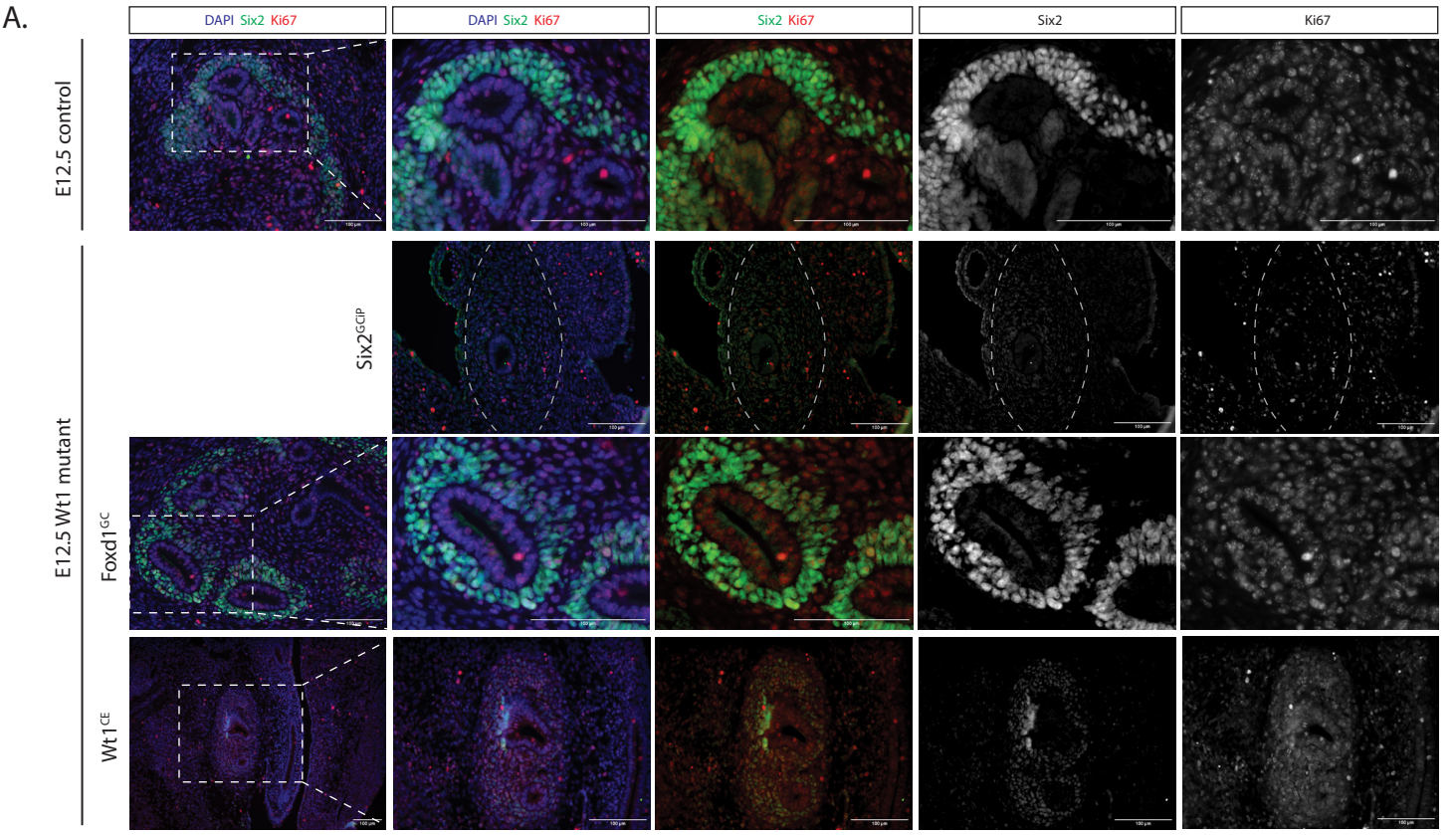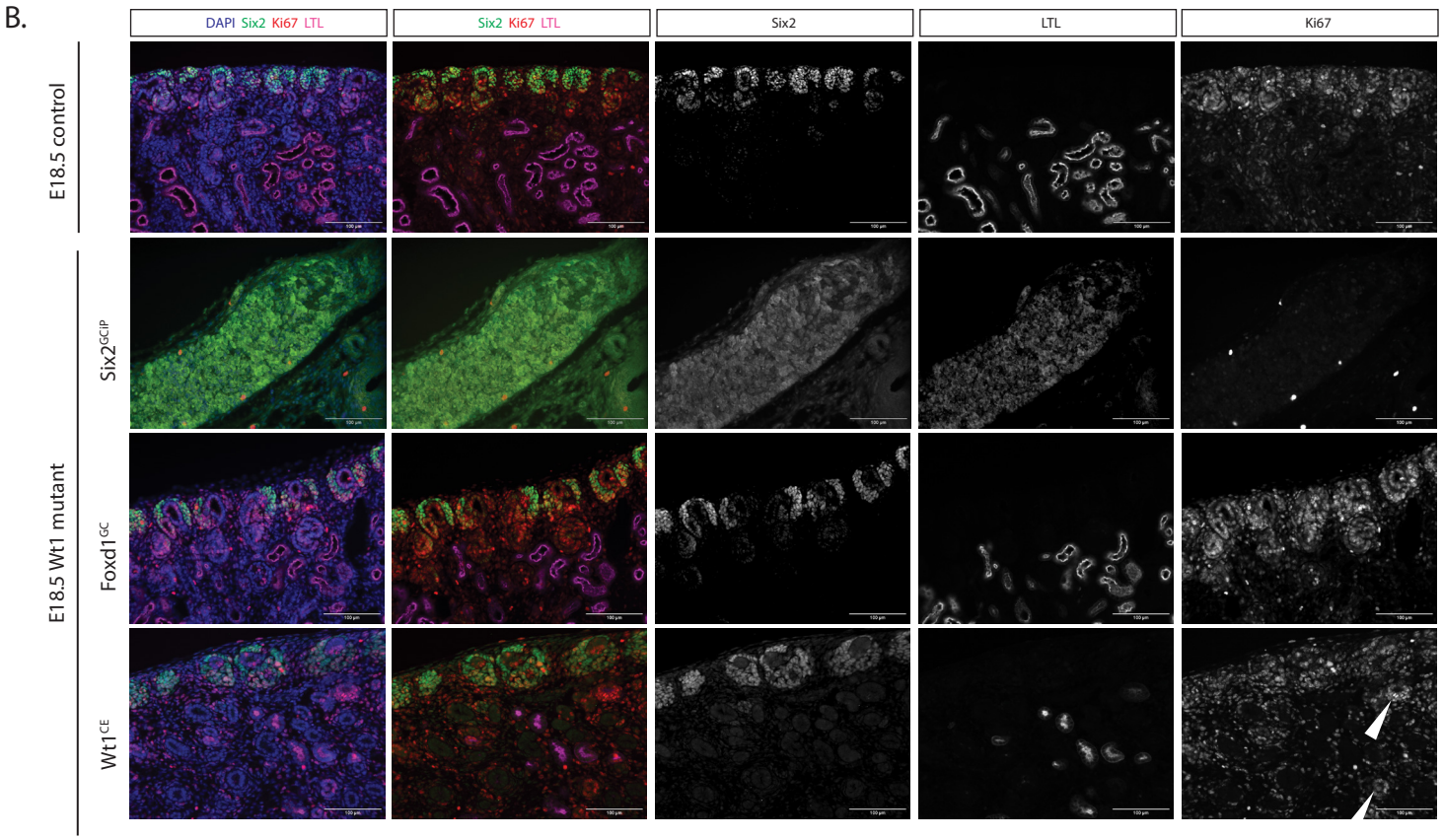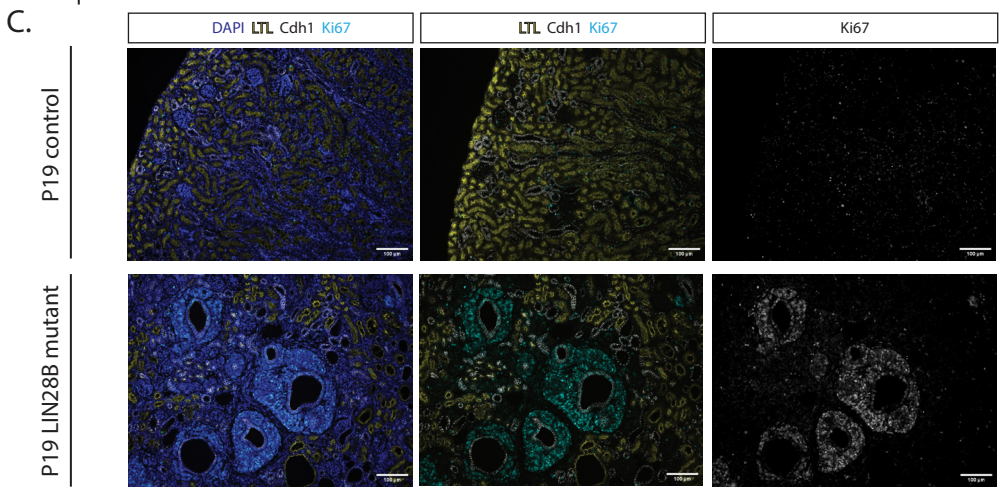
Supplementary Fig. 5